Republic of Iraq
Ministry of Higher Education
And Scientific Research
University of Kerbala
College of Science / Department of Physics

Nuclear Structure Study for Light Nuclei ^{6}Li , ^{9}Be

A Thesis

Submitted to the College of Science /

University of Kerbala in partial fulfillment

of the requirements for the

degree of Master of Science in Physics

by

Sabaa Majeed Hameed

Supervised by

Prof. Dr. Adie D. Salman

2021 A.D 1442 A.H

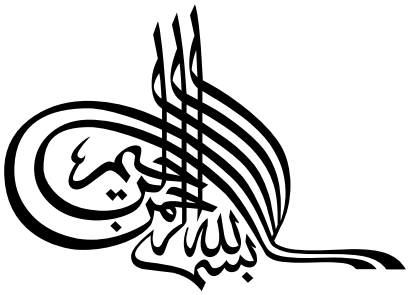

﴿وَعِندَهُ مَفَاتِحُ الغَيْبِ لا يَعلمُها إلا هُو
وَيَعْلَمُ
مَا فِي البَرِّ وَالبَحْرِ وَمَا تَسْقُطُ مِنْ وَرَقَةٍ
إلا يَعْلَمُها وَلا حَبَّةٍ فِي ظُلُماتِ الأَرْضِ
ولا رَطْبٍ وَلا يَابِسٍ إلا فِي
كِتابٍ مُبِينْ﴾

صدق الله العلي العظيم

سورة الأنعام (الآية : ٥٩)

Acknowledgments

Praise be to **Allah**, Lord of the whole creation and peace

be upon his messenger **Mohammed (phuh)**

Oh God, I would like to thank you for this blessing that deserve thanks.

I would like to give special thanks to my supervisor

Prof. Dr. Adie D. Salman

For suggesting this project, his help, guidance, encouragement, the advice throughout the work and for many helpful discussions and suggestions.

I wish I had a word better than thanks to express my feeling to my father, mother, and to all my family.

I would like to thank the Head and the staff of the department of Physics for all the assistance they gave. My thanks also extend to the dean of the College for his support to perform this work.

I would like to acknowledge everyone who has contributed to the success of this thesis, whether directly or indirectly. I thank everyone asked God for my success.

Abstract

The large basis no-core model has been applied in ^{6}Li and ^{9}Be nuclei, to study the structure and some electromagnetic properties of these nuclei. The shell model calculation included two models-space psd and spsdpf with psdmwk and wbm interactions respectively.

According to the psd and spsdpf model space, the one-body density matrix element was calculated and used to check the elastic and inelastic form factors and energy levels for the low-lying excited state of these nuclei. The single-particle radial wave function adopted Wood-Saxon and Skyrme (Sly4) potentials.

The psd model-space calculated energy level is in a reasonable agreement with the experimental results at the lowest energy band (positively parity levels), while the higher band (negative parity levels) is shown greater value than the experimental data with about 2-12 MeV.

The shell model calculation used the large-basis consists of four shells (1s, 1p, 1d-2s, 1f-2p) truncated to (0+2) ħω which is enough convergence for these states because the expansion to 4 and 6 ħω give only a slight change in energy levels of the higher shell only. The large-basis calculation for the even parity energy level agreed well with the experimental results for both nuclei.

The elastic and inelastic form factors were calculated for the low-lying excited state of both nuclei using Skyrme (sly4) potential which shows good agreement with experimental data compared with that of wood-Saxon.

Contents

List of Symbol

spsdpf	Models space included $1s_{1/2}$, $1p_{3/2}$, $1p_{1/2}$, $1d_{3/2}$, $1d_{5/2}$, 2s1/2, $1f_{7/2}$, $1F_{5/2}$, $2P_{3/2}$, $2P_{1/2}$ orbits
psd	Models space included $1p_{1/2}$, $1p_{3/2}$, $1d_{3/2}$, $1d_{5/2}$, $2s_{1/2}$ orbits
wbm	Effective interactions for the 1p2ls1d nuclear shell-model space.
sly4	Skyrme effective interactions type
Ws5	Wood-Saxon potential
$a_{so} = a_{o.}$	Surface diffuseness parameter for both the central and spinorbit potential = 0.65 fm.
Vo(r)	The spin-independent central potential.
r_c	the radius is a little smaller with r_c = 1.20 fm.
θ	The scattering angle in laboratory coordinates.
E_i	The total energy of the initial incident electron.
E_f	The final total energy of the scattered electron.
t_0 , t_1, t_3	The coefficients of the isospin-coupled Sachs of the nucleons
$F_J(q)$	Nuclear form factor
$V_{so}(r)$	The spin-orbit potential.

Chapter One

Chapter one

General Introduction

1.1 Introduction

The shell model is one of the most basic nuclear models which is used in the study of nuclear structure and nuclide properties. [1] This model can be compared with the electron shell model for atoms, as atomic behavior and properties can be described with valance electrons which exist out of a closed shell, likewise, valance nucleons (protons or neutrons) in a nucleus which are placed out of close shells (with magic numbers 2,8,20,28,50,82 and 126) play important roles to determining nuclear properties. In the shell model, the nucleons (protons and neutrons) have detached energy levels, these energy states have certain angular momentum. When the nucleus is at the ground level, its protons will be in the lowest probable energy state. A nucleus of unusual stability are formed when its shells of protons or neutrons are full. In this case, the number of protons or neutrons is known as a magic number. Nuclei with these numbers are very stable and have completely different properties compared with their neighbors. [2]

In the p-shell model space, the valence nucleon occupies $1P_{3/2}$ $1P_{1/2}$ outside the ^{4}He core. This model failed to reproduce the form factors and the transition rate without using scaling factors or insert the effect of the higher configuration (core-polarization) into account. The higher configuration means in the p-shell nuclei that including excitation of nucleons from $0s_{1/2}$ to higher allowed orbits. [3]

1.2 Shell model

In the study nuclear structure has been made by the development of nuclear shell-model.This model, although simple, it has led to the explanation of many nuclear properties such as spin, magnetic moment, and nuclear spectra. The basic hypothesis of the nuclear shell model is that the first approximation each nucleon moves separately in a potential that represents that average interaction with the other nucleons in the nucleus.This unconnected motion of the nucleons can recognize qualitatively from a federation of the weakness for the nuclear long-range attraction and the Pauli Exclusion Principle. [4]

The nucleus is conceptualized as being composed of filling shells that contain the maximum number of neutrons and protons allowed by the Pauli exclusion principle and unfilled shells containing the remaining number of neutrons and protons to form the specific nucleus. [5] A shell model assumes that the properties of the nucleus are determined by the last unpaired nucleon and the valence nucleons occupy a selected set of single-particle levels (called model space).[6] The single-particle wave function obtained from either Woods-Saxon (WS) or Skyrme potential (sly4)combined with these matrix elements of the one-body operators to create model space transition densities.

1.3. Electron Scattering

The electron scattering has been utilized widely using as a probe to the nuclear structure. When the electron is at high energy (in the 100MeV or higher), it scattered with the de-Broglie wavelength associated with the order of few Fermi, which is equal to or smaller than the radius of the nucleus. [5]

The electron dispersion is divided into two types:

a- The elastic electron dispersion

The electron is scattering leaving the nucleus at its ground states and the energy of the electron unchanged [8]. which studies the ground state properties such as static distributions of charge and magnetization [9].

b- Inelastic electron scattering

An electron is scattered from the nucleus, leaving the nucleus in an excited state and its final energy decreases from the initial amount that the nucleus takes in. [8] The inelastic scattering of electrons proved an excellent way to explore the nuclear structure [9]. Measuring the cross-section of the electrical excitation allows getting nuclear dynamic properties such as the charge distributions and current densities [9].

Theoretical work on electrons scattering from the nuclei of the charge-Ze began by Mott (1929).[10] In this work the nuclear size can be taken into the calculation by multiplying the Motts cross-section by a factor depending on the charges, current and magnetization distribution in the target nucleus, and this factor is called the nuclear form factor. [6] The interaction of an electron with the nucleus can be described according to the first Born approximation, which considers the initial and final states of the electron as pure plane waves, such as the exchange of a virtual photon carrying angular momentum of 0 or ± 1 along the direction of q. [8,11] The Born approximation is only valid under $z\alpha << 1$, where z is the atomic number and α is the fine structure constant.

The form factor is divided into two types, according to the first Born's approximation:

1- Coulomb form factor:

The longitudinal form factors are defined as the interaction of the electron with the charge distribution of the nucleus in the first Born approximation's as an exchange of the virtual photon carries zero angular momentum with a long q direction. The longitudinal form factor (Coulomb) is represented as a Fourier transform of the charge density [12].

2-Transverse form factor

The interaction of the electron with the current distribution of the nucleus in which the virtual photon carries angular momentum ±1 a long q direction is called a transverse form factor. The transverse form factor is represented as the Fourier transform of the current density. The transverse form factor is divided into electric (E) and magnetic (M) according to the parity and angular momentum selection rules. [12]

1.4 Literature Review

Many attempts were made to explain the experimental data of electron scattering and to understand the nature of nuclear force and the structure of the nuclei in Li and Be nuclei. Kelly (1991)[13] has investigated the structure of ^{9}Be using electron scattering measurements, and the used detailed line-shape analysis extract cross-sections for broad states. Booten and van Hees (1994) [14] calculated the transverse electron scattering form factors of states in several selected p-shell nuclei. The shell model calculations have been included 0p-shell and extended (0+2) $h\omega$ model space. The inclusion of the meson exchange current improved the agreement of the transverse form factor with experimental results.

Kukulin et al. (1995) [15] described all the low states of the nucleus A = 6 (^{6}He, ^{6}Li, ^{6}Be) in terms of a realistic three-body model α+2N using soft-core NN full Reid potential (RSC). This model which included a different type of force (central, tenser, spin-orbit, Coulomb) failed to calculate the quadrupole moment values. Karataglidis et al. (1996) [16] calculated the elastic and inelastic electron scattering for ^{6,7}Li nuclei using shell model wave function 0$h\omega$ space to (0+2+4+6) $h\omega$. These calculations showed a decrease in the magnetic momentum values with higher excitation to (0+2+4+6) hω. Zeina (2003)[17] calculated the inelastic longitudinal C2 form factors of the similar parity states of ^{6}Li,^{7}Li,^{10}B and ^{12}C in the framework of the many-particle shell model. In this model a core of ^{4}He is being assumed and the remaining particles are distributed over $1p_{3/2}$ and $1p_{1/2}$ orbits which form the model space. The calculation result with inclusion of the core- polarization using the Tassie model gave an acceptable result with the experimental data in the region $q \leq 3$ fm-1.

Adie (2005)[18] studied the longitudinal and transverse electron scattering form factors in some p-shell nuclei taking into account core-

polarization effects up to second order. The inclusion of the second-order core-polarization effects improve the calculated results by a little amount to both the transition strength and longitudinal form factors.

Laith (2006) [19] studied the transverse electron scattering form factors of low-lying excited of the ^{6,7}Li nuclei. Their results computed using effective g-factor gave good agreement with the experimental data.

Khalid (2007) [20]calculated the elastic and inelastic electron scattering form factors in light nuclei (^{6}Li,^{7}Li,^{9}Be,^{10}B,^{11}B,^{12}C,^{13}C and ^{15}N)used Nucleon-Nucleon(NN) interaction. Higher energy excitation from 1s-shell core orbits and also from the valence 1p-shell to higher allowed orbits up to $2\hbar\omega$ is considered for core-polarization calculations. They used the Cohen-Kurath interaction for the 1p-shell model space. The calculation forms factors, especially the Coulomb scattering gave good agreement with experimental data while the magnetic form factors were less affected.

Radhi et al.(2014) [21] calculated the Quadrupole moments and effective charges for Li (A = 7, 8, 9, 11) and B (A = 8, 10, 11, 12, 13, 14, 15) isotope based on the shell model with p and large basis spsdpf-shell model spaces. Effective charges are obtained for the neutron-rich Li and B isotopes, which are smaller than the standard values for the stable p- and sd-shell nuclei.

Radhi et al. (2016) [22] studied the nuclear structure of ^{19}F nuclei using shell model and Hartree-Fock calculations they used two different model spaces are the full sd-model space and the large-basis spsdpf-shell space. The Hartree-Fock mean-field method was found appropriate with the shell model for studying the nuclear structure and necessary in obtaining a good agreement.

Radhi et al.(2018) [23] calculated the magnetic dipole and electric quadrupole moments for neutron-rich sd-pf cross-shell nuclei. Their results with Core polarization (CP) is essential for obtaining a reasonable description of the electric quadrupole moments and enhance the Coulomb form factors but has no effect on the dipole magnetic moments.
Ali A. Alzubadi et al.(2018) [24] have investigated elastic and inelastic electron scattering form factors, energy levels, and transition probabilities for positive and negative low-lying states in ^{17}O nucleus. They have used psdpn model space for positive parity states and psd model space for negative parity states. For all selected excited states, Skyrme interaction is adopted to generate from them a one-body potential for Hartree-Forck theory of calculating the single-particle matrix elements.

Noor and Adie (2018)[25]calculated the longitudinal and transverse electron scattering form factors of the ^{7}Li nucleus using the large-basis shell model. The calculation result of the large-basis shell model upto (0+2)ħω seemed to be not sufficient for giving the best description of the form factors data,that can be extended to cover the entire p-shell region.

R.B. Wiringa and R. Schiavilla (2018) [26] calculated the longitudinal and transverse form factors and the transition form factors to the first four excited states in ^{6}Li nuclous. The microscopic based on six-body Variational Monte Carlo wave functions used to calculate the form factors and radiative width. The form factors calculated were in good agreement with experimental data at low momentum transfer.

R. A. Radhi (2019) [27] studied the inelastic electron scattering form factors of low-lying excited states in ^{7}Li by using the Skyrme interaction with the inclusion of the core polarization truncated to (0+2)$\hbar\omega$. Their

results were able to describe the form factors well, especially at high momentum.

1.5. Aim of the present work

The present work aims at accomplishing calculations of the shell model for (psd- shell) and (spsdpf-shell) over a large scale with (0+2)hω truncation to investigate lower energy levels and form factors of the nuclei used. The large scale calculation carries out to the low-lying states, using the single-particle of the radial wave function of wood-Saxon(WS) potentials and of Skyrme-Hartree-Fock (SHF) potentials. The core polarization calculation included through the Tessie model using the NuShell code.

Chapter Two

Chapter two

Theoretical bases

2.1. General Theory

Electron scattering is one of the most powerful methods for studying atomic nuclei properties. The ground-state properties such as static charge distribution and magnetization can be studied using an elastic scattering of electrons. Electrons with energies of several hundreds of MeV must be used to determine these values.

In the plane-wave case, the differential cross-section for the scattering of an electron through a solid angle Ω from a nucleus of charge Ze and mass M. The term "Born approximation" is described as [28]

$$\frac{d\sigma}{d\Omega} = \left(\frac{d\sigma}{d\Omega}\right)_{Mott} \eta \sum_{J} \left|F_J(q,\theta)\right|^2 \qquad (2.1)$$

Where $\left(\frac{d\sigma}{d\Omega}\right)_{Mott}$ is the Mott scattering cross-section which is given by [28]

$$\left(\frac{d\sigma}{d\Omega}\right)_{Mott} = \left[\frac{Z\alpha\cos(\theta/2)}{2E_i\sin^2(\theta/2)}\right]^2 \qquad (2.2)$$

Where $\alpha = e^2/\hbar c = (1/137)$ is the fine structure constant, Z is the target nucleus's atomic number, θ is the scattering angle, and E_i is the incident electron's energy. [29]

Where η is the nucleus' recoil factor, which is calculated as follows:

$$\eta = \left[1 + \frac{2E_i}{M}\sin^2(\theta/2)\right]^{-1} \qquad (2.3)$$

where M is the mass of the target. [30]

The total of the longitudinal and transverse form factors of a given multipolarity J. [31,32]:

$$\left|F_J(q)\right|^2 = \left(\frac{q_\mu}{q}\right)^4 \left|F_J^L(q)\right|^2 + \left[\frac{q_\mu^2}{2q^2} + tan^2(\theta/2)\right] \left|F_J^T(q)\right|^2 \qquad (2.4)$$

$$q^2 \approx 4E^2\eta \sin^2\frac{\theta}{2}$$

The three-momentum transfer and the four-momentum transfer is

where $\omega^2 = E_f - E_i$ is the difference between the final and initial energy.

$q_\mu^2 = q^2 - (E_f - E_i)^2$

The longitudinal (L) and transverse (T) form factors are given by [33]

$$\left|F_J^L(q)\right|^2 = \sum_{J\geq 0} |(q)|^2 \left|F^T(q)\right|^2 \qquad (2.5)$$

$$\left|F_J^T(q)\right|^2 = \sum_{J>0} \left\{\left|F_J^M(q)\right|^2 + \left|F_J^E(q)\right|^2\right\} \qquad (2.6)$$

where $\left|F_J^M(q)\right|^2$ and $\left|F_J^E(q)\right|^2$ are the magnetic and electric transverse form factors, respectively The multipolarity J is determined by the parity selection rules[34]

$|J_i - J_f| \leq J \leq J_i + J_f$

$\pi_i\pi_f = (-1)^J$ for CJ and EJ multiples

$\pi_i\pi_f = (-1)^{J+1}$ for MJ multiples

The electronic scattering Form factors involving angular momentum J can be expressed as [35]:

$$\left|F_J^\Lambda(q)\right|^2 = \frac{4\pi}{z^2}\frac{1}{2J_i+1}\left|\langle\Psi_{Jf}|\hat{T}_J^\Lambda(q)|\Psi_{Ji}\rangle\right|^2 \qquad (2.7)$$

where $\hat{T}_J^\Lambda(q)$ is the electron scattering multiply operator and Λ selects the longitudinal, transverse electric and transverse magnetic form factors [36]:

$$\left|F_J^L(q)\right|^2 = \frac{4\pi}{z^2}\frac{1}{2J_i+1}\sum_{J\geq 0}\left|\langle J_f\, M_{Jf}|\hat{T}_J^{coul}(q)|J_i\, M_{Ji}\rangle\right|^2 \qquad (2.8)$$

$$\left|\mathrm{F}_J^{\mathrm{T}}(\mathrm{q})\right|^2 = \frac{4\pi}{\mathrm{z}^2}\frac{1}{2\mathrm{J_i}+1}\Sigma\{\left|\langle \mathrm{J_f\ M_{Jf}}|\hat{\mathrm{T}}_{\mathrm{J}}^{\mathrm{el}}(\mathrm{q})|\mathrm{J_i\ M_{Ji}}\rangle\right|^2 + |\langle \mathrm{J_f\ M_{Jf}}|\hat{\mathrm{T}}_{\mathrm{J}}^{\mathrm{mag}}(\mathrm{q})|\mathrm{J_i}\, M_{Ji}\rangle|^2\} \quad (2.9)$$

Where J_i and J_f are spins of the initial and final states and the multipole operator are defined by [36]

$$\hat{\mathrm{T}}_{\mathrm{J}}^{\mathrm{coul}}(\mathrm{q}) = \int \overrightarrow{dr}\, j_J(qr) Y_J^M(\Omega_r)\hat{\rho}(\vec{r}) \quad (2.10)$$

$$\hat{\mathrm{T}}_{\mathrm{J}}^{\mathrm{el}}(\mathrm{q}) = \frac{1}{q}\int \overrightarrow{dr}\{\vec{\nabla}\times\left[j_J(qr)Y_{JJ_1}^M(\Omega_r)\right]\}.\hat{J}(\vec{r}) \quad (2.11)$$

$$\hat{\mathrm{T}}_{\mathrm{J}}^{\mathrm{mag}}(\mathrm{q}) = \int \overrightarrow{dr}\left[j_J(qr)Y_{JJ_1}^M(\Omega_r)\right].\hat{J}(\vec{r}) \quad (2.12)$$

Where $j_J(qr)$ is the spherical Bessel function, $(\hat{J}(\vec{r}), \hat{\rho}(\vec{r}))$ are the current and charge density operators for the target, and the $Y_{JJ_1}^M$ is the vector spherical harmonic, given by [6],

$$\rho(\vec{r}) = \delta(r_i - r)e_i \quad (2.13)$$

$$\hat{J}(\vec{r}) = \delta(r_i - r)e_i\frac{1}{M_T}\vec{\nabla} \quad (2.14)$$

$$Y_{JJ_1}^M(\Omega_r) = \sum_{mm`}(Jm^1m`/JM)Y_{J_1}^M(\Omega_r)\, e_i \quad (2.15)$$

With, $e_i = \frac{(1+\tau_z(i))}{2}$ (the nucleon charge), $\tau_z = 2t_z$,and $\delta(r_i - r)$ is Dirac delta function, and, $Y_{J_1}^M(\Omega_r)$ is the spherical harmonic function.

2.2. Corrections to the form factor

The measured form factor will be subjected to two corrections, the first of which is the center of mass correction. Due to the fact that the interaction potential represents an average potential with respect to a fixed origin, where the Hamiltonian can be separated into two sections, one represents the motion of the center of mass and the other represents the intrinsic m, the shell model wave functions used to describe transition densities have given rise to additional non-physical excited states called spurious states.[32]

The center of mass correction is given as [37]

$$F_{c.m} = \frac{q^2 b^2}{4A} \qquad (2.16)$$

where A is the mass number and b is the harmonic oscillator size parameter. The second correction is the inclusion of finite nuclear size in the calculation, the finite nucleon-size correction, as follows [38]

$$F_{f.s}(q) = \left[1 + \left(\frac{q}{4.33}\,\mathrm{fm}^{-1}\right)^2\right]^{-2} \qquad (2.17)$$

Except in the region of the diffraction minima, where the PWBA goes to zero, the plane wave Born approximation (PWBA) is expected to characterize the electron scattering data very well for nuclei in which αZ«1. The electrons' Coulomb distortion raises q, and these effects can be accounted for using an efficient momentum transfer. The effective momentum transfer is calculated as follows: [39]

$$q_{eff} = q\left[1 + \frac{3\,ze^2}{2E_i R_c}\right] \qquad (2.18)$$

Where $R_c = (\frac{5}{3})^{1/2} R_{rms}$ and R_{rms} is the root mean square (rms) charge radius and $e^2 = \alpha\hbar c = 1.44\mathrm{MeV\ fm}$

These corrections are included in the electron scattering longitudinal and transverse form factors, including angular momentum J and momentum transfer q between the initial and final nuclear shell model states of spin and isospin. [40],

$$\left|F_J^{\Lambda}(q)\right|^2 =$$

$$\frac{4\pi}{z^2(2J+1)}\left|\sum_{T=0,1}(-1)^{T_f-T_Z}\begin{pmatrix} T_f & T & T_i \\ -T_Z & 0 & T_Z \end{pmatrix}\langle J_f T_f \|\|T^{\Lambda}(q)\|\|J_i T_i\rangle\right|^2 \times$$

$$|F_{f.s}F_{c.m}|^2 \qquad (2.19)$$

2.3 Many-Particle Matrix Elements

A microscopic theory blends shell-model wave functions and configuration with higher energy as particle-hole perturbation expansion to explain the effect of core polarization on shape factors. The fp-model space (p) contribution and the core-polarization (cp) contribution are added together to form the reduced matrix part of the electron scattering operator$\widehat{T}_J$.

The p-model space (p) contribution and the core-polarization (cp) contribution are added together to form the reduced matrix part of the electron scattering operator $\widehat{T}_J$ [41].

The electron scattering operator for initial and final wave function is indicated as the collecting over the one-body density matrix element-time the reduce single-particle element and writing as

$$\langle J_f \left\|\widehat{T}_J(q)\right\|J_i\rangle = \langle J_f \left\|\widehat{T}_J(q)\right\|J_i\rangle_{ms} + \langle J_f \left\|\delta\widehat{T}_J(q)\right\|J_i\rangle_{cp} \qquad (2.20)$$

The p-shell model-space matrix elements are expressed as the sum of the product of the One-Body Density Matrix elements (OBDM) times the single-particle matrix elements, which are given by[42]:

$$\langle \mathrm{J_f} \left\| \widehat{\mathrm{T}}_{\mathrm{J}}(\mathrm{q}) \right\| \mathrm{J_i} \rangle =$$

$$\sum_{F_\alpha F_\beta} OBDM\left(\mathrm{J_f J_i} F_\alpha F_\beta J\right) \langle F_\alpha \left\| \widehat{\mathrm{T}}_{\mathrm{J}}(\mathrm{q}) \right\| F_\beta \rangle \qquad (2.21)$$

Where F_α and F_β refers to the initial and final model space states, respectively. The one body density matrix element in the proton-neutron formalism is given by:[42]

$$\mathrm{OBDM}(p/n) = (-1)^{Jf-JZ} \begin{pmatrix} J_f & 0 & J_i \\ -J_Z & 0 & J_Z \end{pmatrix} \sqrt{2}\, \frac{OBDM(J=0)}{2}$$

$$(+/-)\tau Z (-1)^{Jf-JZ} \begin{pmatrix} J_f & 1 & J_i \\ -J_Z & 0 & J_Z \end{pmatrix} \sqrt{6}\, \frac{OBDM(J=1)}{2} \qquad (2.22)$$

$$\mathrm{OBDM}\left(\mathrm{J_f J_i} F_{\alpha,t_z} F_{\beta,t_z} J\right) = \frac{\langle J_f T_f \left\| \left[a^\dagger_{F_\alpha t_z} \otimes \tilde{a}_{F_\beta t_z} \right]^J \right\| J_i T_i \rangle}{\sqrt{2J+1}\sqrt{2T+1}} \qquad (2.23)$$

where $tz = 1/2$ for neutron and $tz = -1/2$ for a proton.

The operators ($a^\dagger$) generate a neutron or proton in the single nucleon state (F_{α,t_z}) and ($\tilde{a}$) remove a neutron or proton in the single nucleon state (F_{β,t_z}). The OBDM used in this study can be deduced from the work of the code Nushell.

2.4.The Woods-Saxon potential

In the Hartree-Fock theory, the Woods-Saxon potential is a convenient phenomenological choice for the one-body potential. It is a model for the properties of single-particle wave functions in the bound-state and continuum states. Since it isn't dependent on a particular two-body interaction, the Woods-Saxon potential (or any other one-body potential) can't be used to calculate the total binding energy. The Woods-Saxon parameters are chosen to better match the energies and radii of nuclear single particles. A spin-independent central potential, a spin-orbit potential, and the Coulomb potential combine to form the Woods-Saxon potential.[43]

$$\mathrm{V(r)} = \mathrm{V}_o f_o(r) + \mathrm{V}_{so}(r)\vec{\ell}.\vec{s} + V_c(r) \qquad (2.24)$$

where $\mathrm{V}_o f_o(r)$ is the spin-independent central potential with a Fermi shape

$$f_o(r) = \frac{1}{1 + \left[exp(r - R_o)/a_o\right]} \qquad (2.25)$$

$\mathrm{V}_{so}(r)$ is the spin-orbit potential

$$\mathrm{V}_{so}(r) = \mathrm{V}_{so}\frac{1}{r}\frac{df_{os}(r)}{dr} \qquad (2.26)$$

with $$f_{so}(r) = \frac{1}{1+\left[exp(r-R_{so})/a_{so}\right]} \qquad (2.27)$$

$V_c(r)$ is the Coulomb potential for protons determined from the Coulomb potential for a sphere with a radius R_c:

$$V_c(r) = \frac{Ze^2}{r} \quad for\ r > R_c \qquad (2.28)$$

and

$$V_c(r) = \left[\frac{3Ze^2 - v}{2R^2{}_c}\right] for\ r < R_c \qquad (2.29)$$

Since the average proton-neutron potential is greater than the average neutron-neutron (or proton-proton) potential, protons can experience a stronger potential than neutrons in nuclei with a neutron surplus. As a result, we'll take:

$$V_{op} = \mathrm{V}_o + \frac{(N-Z)}{A} V_1 \qquad for\ protons \qquad (2.30)$$

$$V_{on} = \mathrm{V}_o - \frac{(N-Z)}{A} V_1 \qquad for\ neutrons \qquad (2.31)$$

theoretically, R_o and a_o for proton and neutrons in a nucleus with $N \neq Z$ could differ slightly. As a consequence, there may be six parameters in the spin-independent potential (and even more if any of them are allowed to take some additional mass dependence). The values of these parameters have been chosen to provide a detailed account of the observed data.

electron scattering-type factors, rms charge radii, and single-particle energies.[43]

2.5. The Skyrme potential

The standard Skyrme force consists of central, tensor and spin-orbit interaction, given by [44]

$$V_{skyrme} = \hat{V}^{central} + \hat{V}^{tensor} + \hat{V}^{LS} \quad (2.32)$$

The central two body Skyrme interaction given by [44]

$$\hat{V}^{central}(r_1, r_2) = \frac{1}{2}t_0\left(1 + \chi_0\hat{P}_\sigma\right)\delta(r_1 - r_2) + \frac{1}{2}t_1\left(1 + \chi_1\hat{P}_\sigma\right)\left[\hat{k}'^2\delta(r_1 - r_2) + \delta(r_1 - r_2)\hat{k}^2\right] + t_2\left(1 + \chi_2\hat{P}_\sigma\right)\hat{k}' \cdot \delta(r_1 - r_2)\hat{k} + \frac{1}{6}t_{31}\left(1 + \chi_{31}\hat{P}_\sigma\right)\rho_0^{\alpha 1}(R) + \frac{1}{6}t_{32}\left(1 + \chi_{32}\hat{P}_\sigma\right)\rho_0^{\alpha 2}(R) \quad (2.33)$$

where $\hat{P}_\sigma = \frac{1}{2}(1 + \hat{\sigma}_1 \cdot \hat{\sigma}_2)$ is the spin-exchange operator, $\hat{k} \equiv \frac{1}{2i}(\nabla_1 - \nabla_2)$ is the relative momentum operator acting to the right and $\hat{k}'$ is the complex conjugate acting to the left, and $\rho_0(R)$ is the isoscalar density at $R \equiv \frac{1}{2}(r_1 - r_2)$. The spin orbit part is given by [45]

$$\hat{V}^{LS}(r_1, r_2) = i\omega_0(\hat{\sigma}_1 + \hat{\sigma}_2) \cdot \hat{k}' \times \delta(r_1 - r_2)\hat{k} \quad (2.34)$$

and the last term is the tensor part [46]:

$$\hat{V}^{tensor}(r_1, r_2) = \frac{1}{2}t_e\{[3(\sigma_1.k')(\sigma_2.k') - (\sigma_1 \cdot \sigma_2)k'^2]\delta(r_1 - r_2) + \delta(r_1 r_2)[3(\sigma_1.k)(\sigma_2.k) - (\sigma_1 \cdot \sigma_2)k^2]\} + \frac{1}{2}t_0\{[3(\sigma_1.k)\delta(r_1 - r_2)(\sigma_2.k) - (\sigma_1 \cdot \sigma_2)k' \cdot \delta(r_1 - r_2)k] + [3(\sigma_2.k')\delta(r_1 - r_2)(\sigma_1.k) - (\sigma_1 \cdot \sigma_2)k \cdot \delta(r_1 - r_2)k']\} \quad (2.35)$$

The Skyrme force (sly4) parameters used in this work from [51].

Chapter Three

Chapter Three

3.1 Introduction

The large-basis shell model calculation used four shells (1s, 1p, 1d-2s, 1f-2p) with (0+2) $\hbar\omega$ truncation, which is an adequate convergence for these states. The Nushell code was used the Tessie model in calculating the core polarization effect. [46]The longitudinal and transverse form factors, as well as energy levels, were measured using the spsdpf and psd model spaces and wbm [47] and psdmwk [48] interactions, respectively. The single-particle of the radial wave function of Skyrme-Hartree-Fock (SHF) was used and their results compared with that of Wood-Saxon (WS) potentials.

3.2 The ^{6}Li nucleus:

The ^{6}Li is an especially interesting nucleus because it is the lightest stable nuclei in the p-shell region. For the conventional many-particle shell models, the ^{6}Li nucleus is essentially a three-body system, two valance nucleons distributed over the $1p_{3/2}$-$1p_{1/2}$ shell and presumably inert 4He core. [49]

2.1 Energy levels:

At the lowest energy band, the calculation result with spsdpf model-space truncated to (0+2) $\hbar\omega$ using Warburton-Brown interaction indicates an acceptable agreement with experimental schemes (positive parity levels) except the 3^+ level overestimated the experimental value. The estimated value of the higher band (negative parity levels) is less than the experimental data within 4 MeV limits. The truncation to 4 and 6 only gives a slight shift in energy levels of the higher shell, the truncation to 2 is found to be a sufficient convergence in these states. For the psd model-space, the measured lower energy band is in fair agreement with the experimental results (positively parity levels), while the higher band (negative parity levels) has a higher value than the experimental results, varying between 2 and 12 MeV.

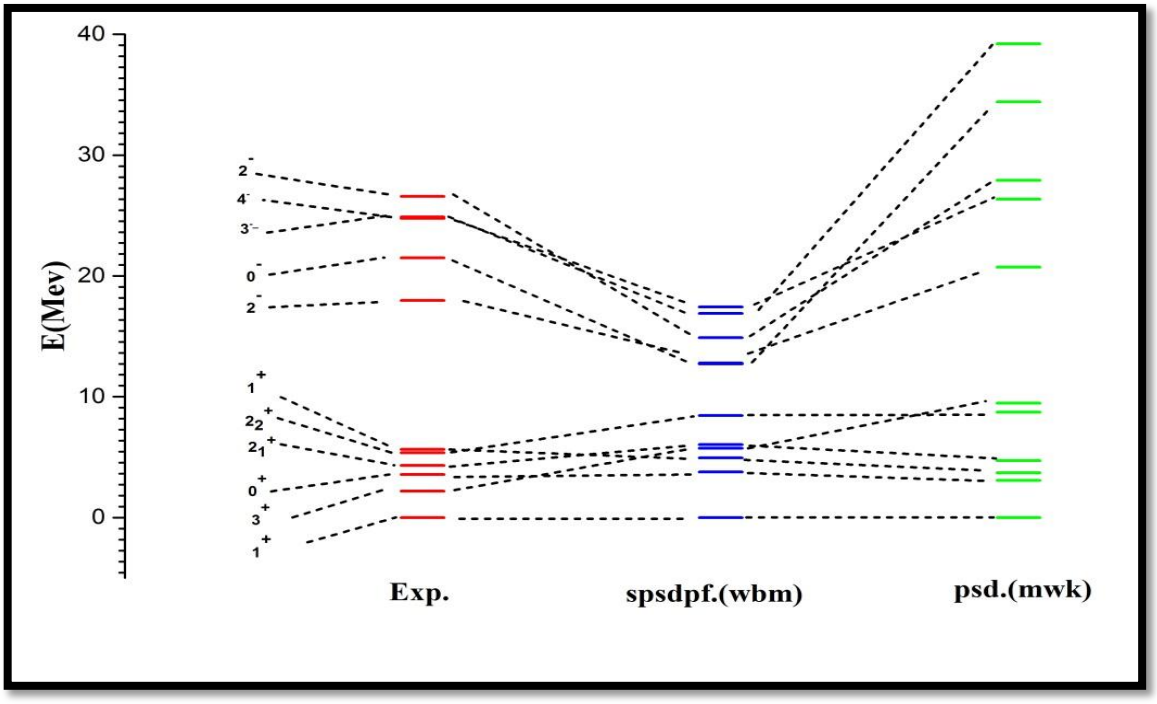

Fig.(3.1): Energy level scheme for the low-lying positive and negative parity states of the ^{6}Li nucleus. The data are taken from ref. [50]

3.2.2 The longitudinal form factor for (1, 0) state

The total longitudinal elastic form factor calculation for the large basis truncation up to (0+2) ħω and individual multipole C0 and C2 contribution is displayed in figure(3.2). The red line curves represented the longitudinal Coulomb total form factors using Wood-Saxon (WS) potentials with effective charge while the blue line without effective charge as shown in figure (3.3). The calculation form factors with bare effective charge (2.2, 0.8) agree well with the experimental data for $q \leq 3.5\ fm^{-1}$. Whereas, the calculation result without effective charge is incompatible with experimental data and falls rapidly at higher momentum transfer. This calculation form factor which uses WS potential didn't show any diffraction minimum behavior.

The One-body density matrix (OBDM) element values for C0 and C2 are displayed in tables (3.1) and (3.2).

Figure (3.4) shows the comparison between both calculation models using WS potential, the spsdpf-shell model space (red solid line) and the psd model space (blue solid line). It is noticed that expanding to a large basis spsdpf gave better results.

The total longitudinal (C0+C2) form factors calculated for spsdpf model space with (0+2) ħω truncation and individual contribution with bare effective charge (3.0, 2.6) displayed in figure (3.5). The result calculation with Skyrme (Sly4) [51] potential showed good agreement with the experimental result and reproduce the diffraction minimum at the correct location (around $q = 2.7 fm^{-1}$). While the results without effective charge underpredict the experimental data at low momentum transfer ($q \leq 1\ fm^{-1}$) and this calculation fails to reproduce the diffraction

minimum structures as shown in figure (3.6). In Fig. (3.5), we see how C0 and C2 are interchanged for influence, where C2 is dominant at the high momentum transfer (q ≥ 1 fm^{-1}).

Table (3.1): The calculated C0 elastic transition OBDM element ($J^{\pi}T = 1^{+}\ 0$) in ^{6}Li nucleus.

^{6}Li		C0
j_i	j_f	OBDM(ΔT=1)
$1s_{1/2}$	$1s_{1/2}$	3.34355
$1s_{1/2}$	$2s_{1/2}$	0.11360
$1p_{3/2}$	$1p_{3/2}$	0.63887
$1p_{3/2}$	$2p_{3/2}$	0.04354
$1p_{1/2}$	$1p_{1/2}$	0.84030
$1p_{1/2}$	$2p_{1/2}$	0.05047
$1d_{5/2}$	$1d_{5/2}$	0.02176
$1d_{3/2}$	$1d_{3/2}$	0.02597
$2s_{1/2}$	$1s_{1/2}$	0.11360
$2s_{1/2}$	$2s_{1/2}$	0.02479
$1f_{5/2}$	$1f_{5/2}$	0.00042
$2p_{3/2}$	$1p_{3/2}$	0.04354
$2p_{3/2}$	$2p_{3/2}$	0.00359
$2s_{1/2}$	$1p_{1/2}$	0.05047
$2s_{1/2}$	$2s_{1/2}$	0.00380

Table (3.2): The calculated C2 elastic transition OBDM element $(J^{\pi}T = 1^{+}\ 0)$ in ^{6}Li nucleus.

^{6}Li		C2
j_i	j_f	OBDM(ΔT=1)
$1s_{1/2}$	$1s_{1/2}$	-0.00105
$1s_{1/2}$	$1d_{3/2}$	-0.00128
$1s_{1/2}$	$2s_{1/2}$	0.00841
$1p_{3/2}$	$1p_{3/2}$	0.46048
$1p_{3/2}$	$1p_{1/2}$	-0.10239
$1p_{3/2}$	$1f_{5/2}$	0.00451
$1p_{3/2}$	$2p_{3/2}$	0.03203
$1p_{3/2}$	$2p_{1/2}$	-0.01347
$1p_{1/2}$	$1p_{3/2}$	0.10239
$1p_{1/2}$	$1p_{1/2}$	-0.12751
$1p_{1/2}$	$2p_{3/2}$	0.01466
$1p_{1/2}$	$2p_{1/2}$	-0.01563
$1d_{5/2}$	$1d_{5/2}$	0.01547
$1d_{5/2}$	$1d_{3/2}$	-0.00637
$1d_{3/2}$	$1s_{1/2}$	0.00128
$1d_{3/2}$	$1d_{5/2}$	0.00637
$1d_{3/2}$	$1d_{3/2}$	-0.00642
$1d_{3/2}$	$2s_{1/2}$	-0.00292
$2s_{1/2}$	$1s_{1/2}$	0.00841
$2s_{1/2}$	$1d_{3/2}$	0.00292
$2s_{1/2}$	$2s_{1/2}$	0.00693
$1f_{5/2}$	$1p_{3/2}$	-0.00451
$1f_{5/2}$	$1f_{5/2}$	0.00035
$1f_{5/2}$	$2p_{3/2}$	-0.00048
$2p_{3/2}$	$1p_{3/2}$	0.03203
$2p_{3/2}$	$1p_{1/2}$	-0.01466
$2p_{3/2}$	$1f_{5/2}$	0.00048
$2p_{3/2}$	$2p_{3/2}$	0.00246
$2p_{3/2}$	$2p_{1/2}$	-0.00155
$2p_{1/2}$	$1p_{3/2}$	0.01347
$2p_{1/2}$	$1p_{1/2}$	-0.01563
$2p_{1/2}$	$2p_{3/2}$	0.00155
$2p_{1/2}$	$2p_{1/2}$	-0.00140

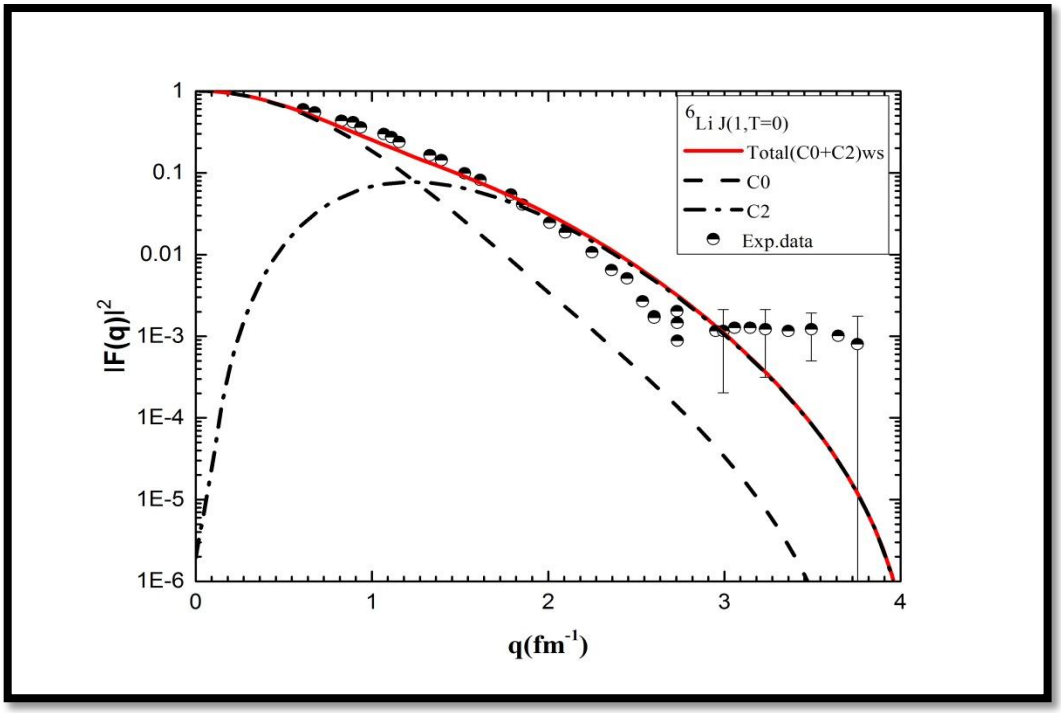

Fig.(3.2): The total longitudinal elastic (C0+C2) and individual multipole form factors for the $J^{\pi}T = 1^{+}\ 0$ state in ^{6}Li nucleus. The calculated form factors using wood-Saxon potential truncated up to (0 + 2) $\hbar\omega$. The data are taken from Refs.[52,53]

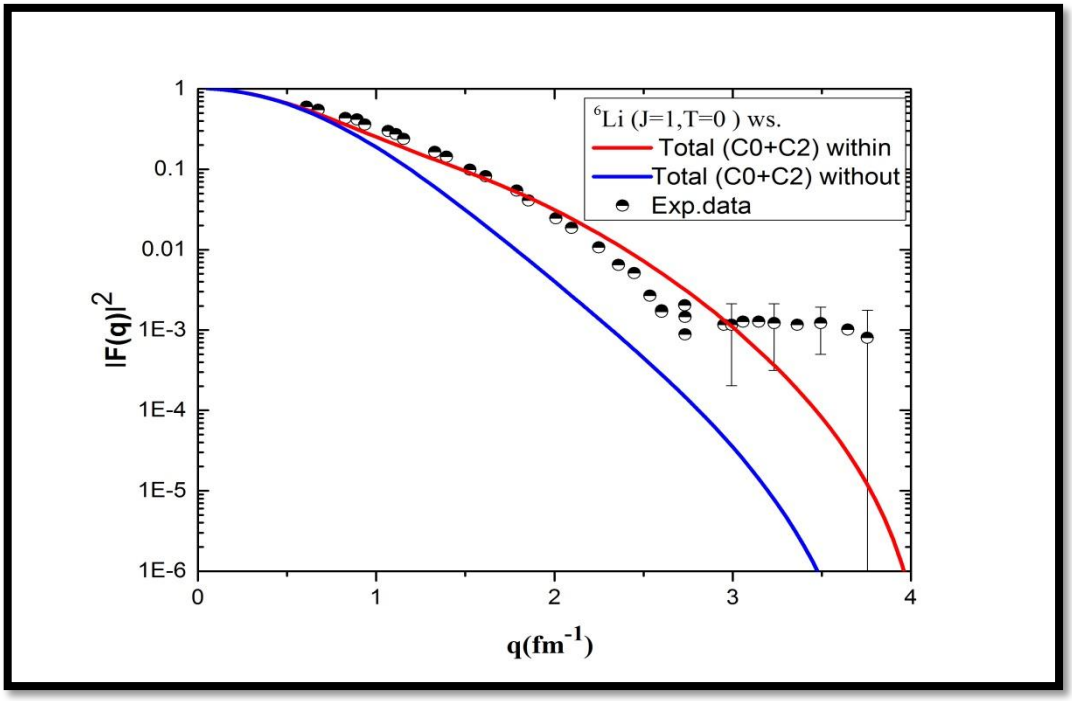

Fig.(3.3): Total longitudinal (C0+C2) elastic form factor calculation for the $J^{\pi}T = 1^{+}\ 0$ state in ^{6}Li truncated to (0+2) ħω with and without effective charge. The experimental data are taken from Refs.[52,53]

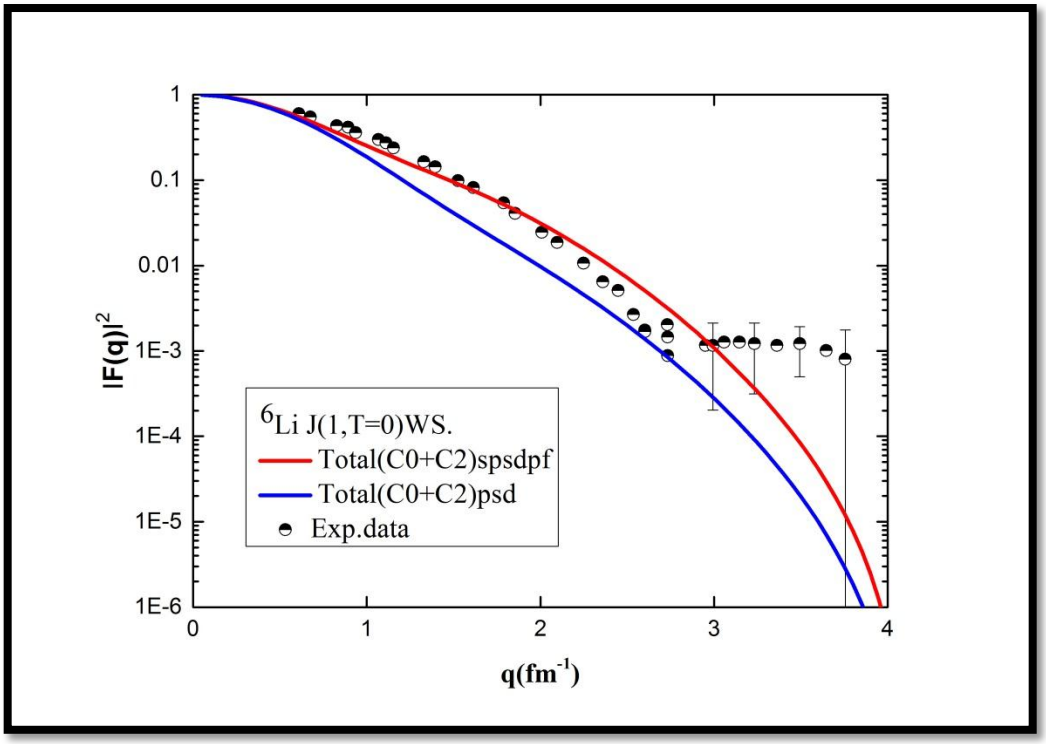

Fig.(3.4): Total longitudinal (C0+C2) elastic form factor for the $J^{\pi}T = 1^{+}\ 0$ state in ^{6}Li calculated with (0+2)$\hbar\omega$ truncated using spsdpf and psd model space. The experimental data are taken from Refs. [52,53]

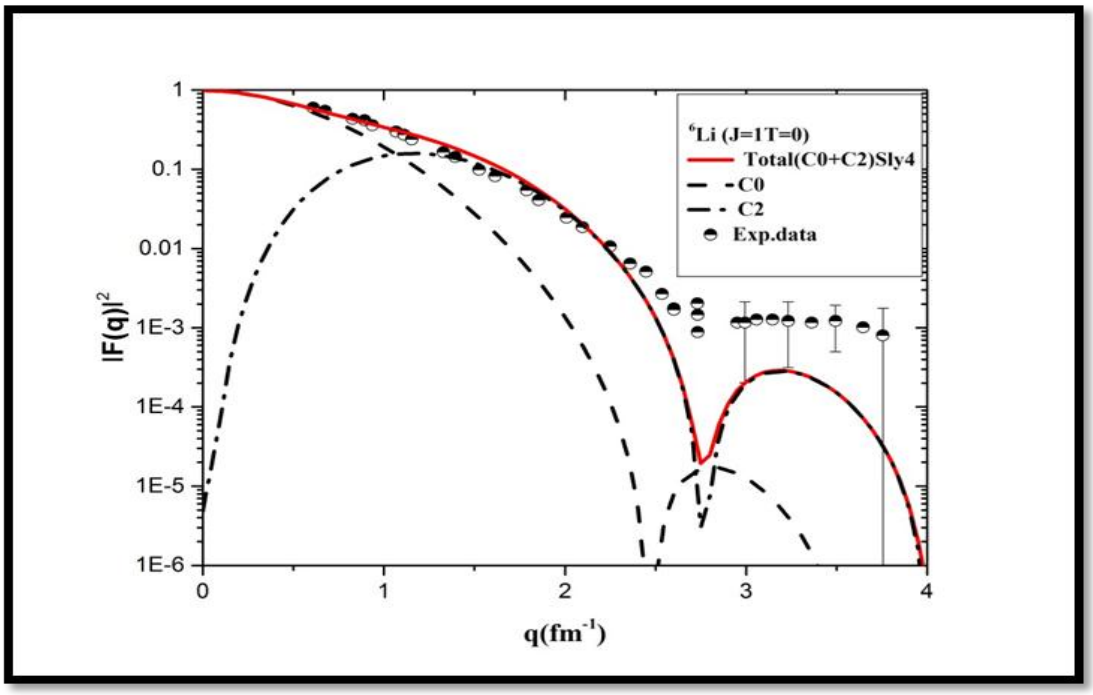

Fig.(3.5): Total longitudinal (C0+C2) elastic form factor and individual multipole for the $J^{\pi}T = 1^{+}\ 0$ state in ^{6}Li calculated with effective charge using Skyrme (sly4) potential. The data are taken from Refs.[52,53]

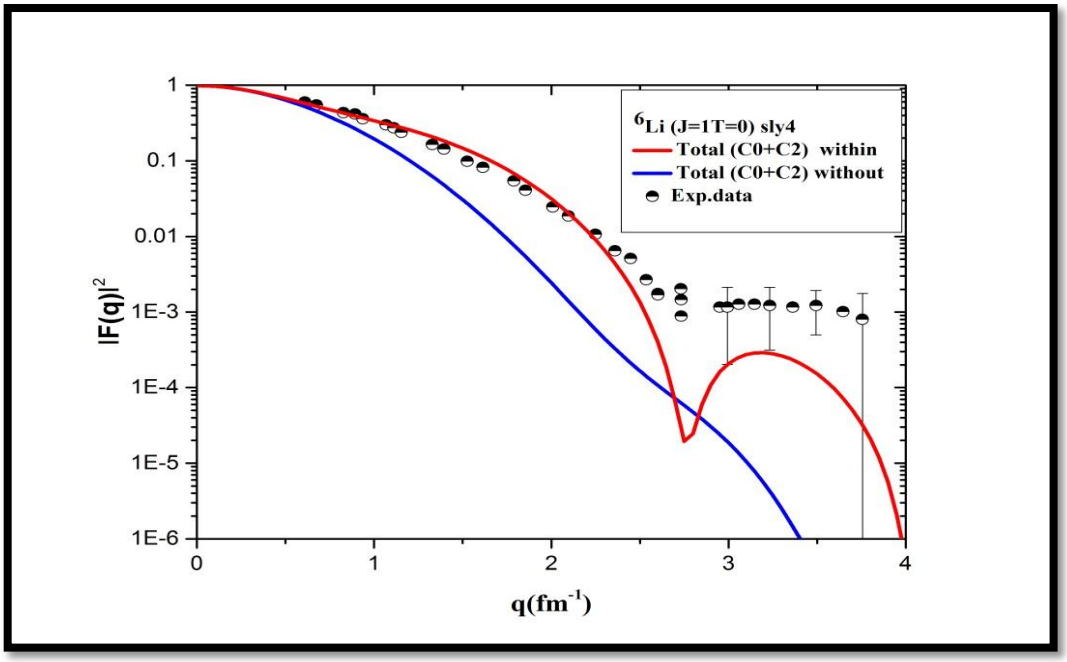

Fig.(3.6): The total (C0 + C2) longitudinal elastic form factor for the $J^{\pi}T = 1^{+}\ 0$ state in ^{6}Li calculated with and without effective charge using Skyrme (sly4) potential. The data are taken from Refs [52,53].

3.2.3 The longitudinal form factor for (3, 0) state

Figure (3.7) shows the total longitudinal inelastic (C2+C4) form factor calculated for the large-basis truncation up to (0+2) ħω using WS potential. The individual longitudinal quadrupole Coulomb (C2) contribution is represented by a dot-line dominates the form factor and shows diffraction minima at $q \geq 4.1\ fm^{-1}$. The total longitudinal form factors with the default (0.35, 0.35) and without effective charge display in figure (3.8). The calculation form factors with default effective charge are reasonably well reproduced the experimental data at $q \leq 3\ fm^{-1}$, while the calculation without effective charge underestimates the experimental data. The One-body density matrix element values for these transitions C2 and C4 are displayed in tables (3.3) and (3.4) respectively.

Figure (3.9) shows the total multipolarity (C2+C4) form factors for spsdpd model and psd model both calculation describes the data very well and shows a diffraction minimum at $q \geq 4.1\ fm^{-1}$.

Figure (3.10) shows the total multipolarity (C2+C4) form factors for large basis calculation using Skyrme (Sly4) potential. The calculation results with default effective charge show a good agreement with experimental data and reproduce the diffraction minimum at the correct place. The quadrupole C2 be in control of the calculation form factor and enhance the agreement with the experimental data.

Figure (3.11) shows the calculation result with the default and without effective charge. The calculation results without effective charge underestimate the experimental data at all momentum transfer and sift the diffraction minimum to higher momentum.

Table (3.3): The calculated C2 transition OBDM element values for $J^{\pi}T = 3^{+}\ 0$ (E_x= 2.186 MeV) in ^{6}Li nucleus.

^{6}Li		**C2**
j_i	j_f	**OBDM (ΔT=0)**
$1s_{1/2}$	$1d_{5/2}$	**-0.00851**
$1s_{1/2}$	$1d_{3/2}$	**-0.02387**
$1p_{3/2}$	$1p_{3/2}$	**0.22342**
$1p_{3/2}$	$1p_{1/2}$	**0.86355**
$1p_{3/2}$	$1f_{5/2}$	**0.00276**
$1p_{3/2}$	$2p_{3/2}$	**0.02162**
$1p_{3/2}$	$2p_{1/2}$	**0.06365**
$1p_{1/2}$	$1p_{3/2}$	**-0.01066**
$1d_{5/2}$	$1s_{1/2}$	**-0.01345**
$1d_{5/2}$	$1d_{5/2}$	**0.00505**
$1d_{5/2}$	$1d_{3/2}$	**0.00898**
$1d_{5/2}$	$2s_{1/2}$	**0.00718**
$1d_{3/2}$	$1s_{1/2}$	**0.01353**
$1d_{3/2}$	$1d_{5/2}$	**0.00119**

$1d_{3/2}$	$1d_{3/2}$	0.00525
$1d_{3/2}$	$2s_{1/2}$	0.00023
$2s_{1/2}$	$1d_{5/2}$	0.00035
$2s_{1/2}$	$1d_{3/2}$	0.00625
$2s_{1/2}$	$1p_{3/2}$	0.01247
$1f_{7/2}$	$1f_{5/2}$	0.00019
$1f_{7/2}$	$2p_{3/2}$	0.00105
$1f_{5/2}$	$1p_{3/2}$	0.00293
$1f_{5/2}$	$1p_{1/2}$	-0.00202
$1f_{5/2}$	$1f_{5/2}$	0.00001
$1f_{5/2}$	$2p_{3/2}$	0.00023
$1f_{5/2}$	$2p_{1/2}$	-0.00001
$2p_{3/2}$	$1p_{3/2}$	0.00331
$2p_{3/2}$	$1f_{1/2}$	0.01307
$2p_{3/2}$	$1f_{5/2}$	0.00004
$2p_{3/2}$	$2p_{3/2}$	0.00035
$2p_{3/2}$	$2p_{1/2}$	0.00103

Table (3.4): The calculated C4 transition OBDM element values for $J^{\pi}T = 3^{+}\ 0$ (E_x= 2.186 MeV) in ^{6}Li nucleus

^{6}Li		C4
j_i	j_f	OBDM(ΔT=0)
$1p_{3/2}$	$1f_{5/2}$	0.01950
$1d_{5/2}$	$1d_{5/2}$	0.00204
$1d_{5/2}$	$1d_{3/2}$	0.00476
$1d_{3/2}$	$1d_{5/2}$	-0.00096
$1f_{7/2}$	$1p_{3/2}$	0.00120
$1f_{7/2}$	$1p_{1/2}$	0.00865
$1f_{7/2}$	$2p_{3/2}$	-0.00005
$1f_{7/2}$	$2p_{1/2}$	0.00049
$1f_{5/2}$	$1p_{3/2}$	0.00472
$1f_{5/2}$	$1f_{5/2}$	0.00003
$1f_{5/2}$	$2p_{3/2}$	0.00032
$2p_{3/2}$	$1f_{5/2}$	0.00032

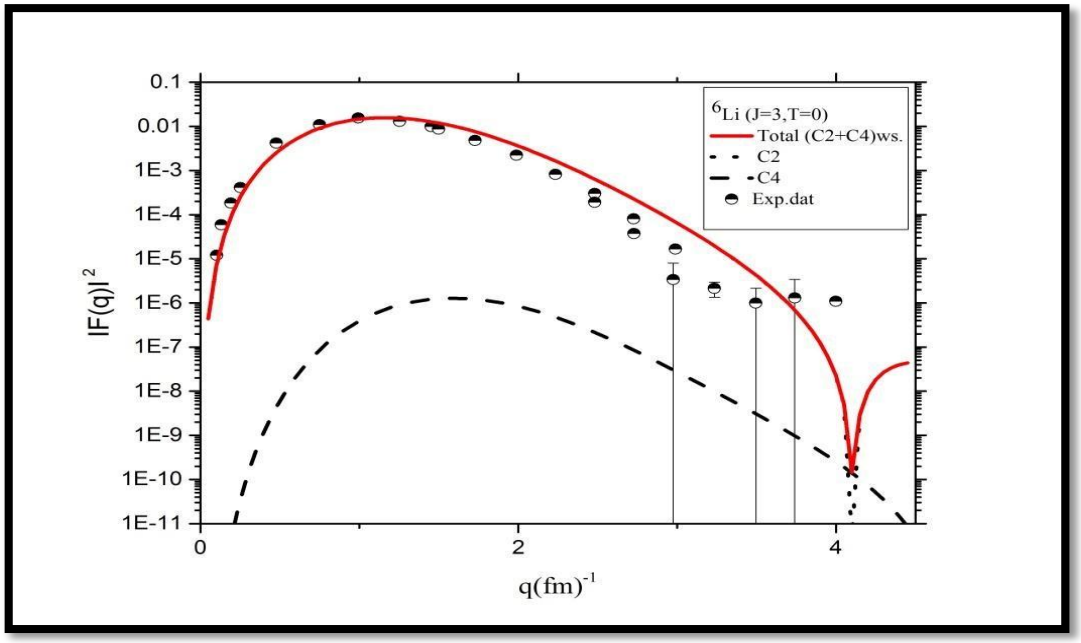

Fig.(3.7).Total (C2 + C4) longitudinal inelastic form factor and individual multipole contribution transition to the $J^{\pi}T = 3^{+}\ 0$ (E_x=2.186MeV) state in ^{6}Li. The experimental data are taken from Refs. [52,53]

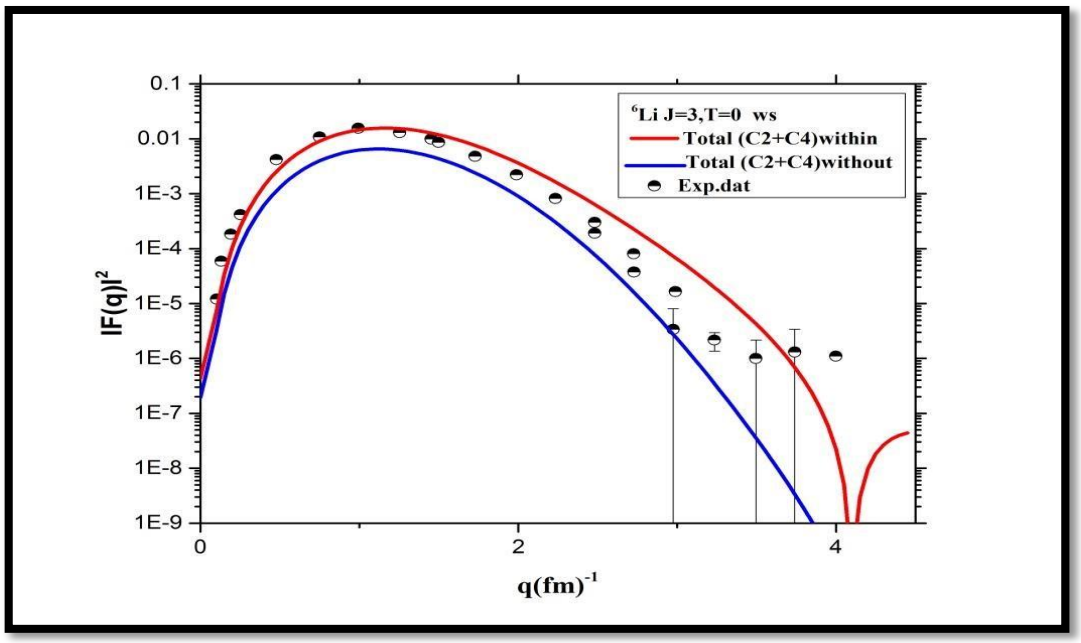

Fig.(3.8) Total (C2 + C4) longitudinal inelastic form factor for the $J^{\pi}T = 3^{+}\ 0$ (E_x=2.186MeV) state in ^{6}Li with and without effective charge using Wood-Saxon potential. The data are taken from Refs. [52,53]

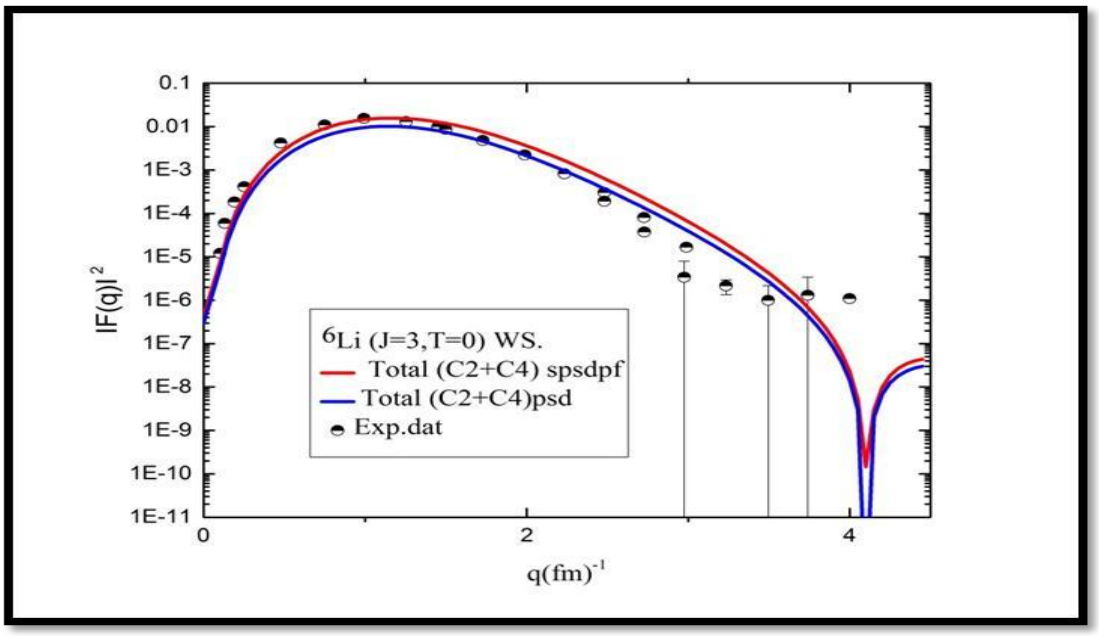

Fig.(3.9): Total longitudinal elastic (C2 + C4) form factor to the $J^{\pi}T = 3^{+}\ 0$ (E_x=2.186MeV) state in ^{6}Li using spsdpf and psd model space. The data are taken from Refs. [52,53]

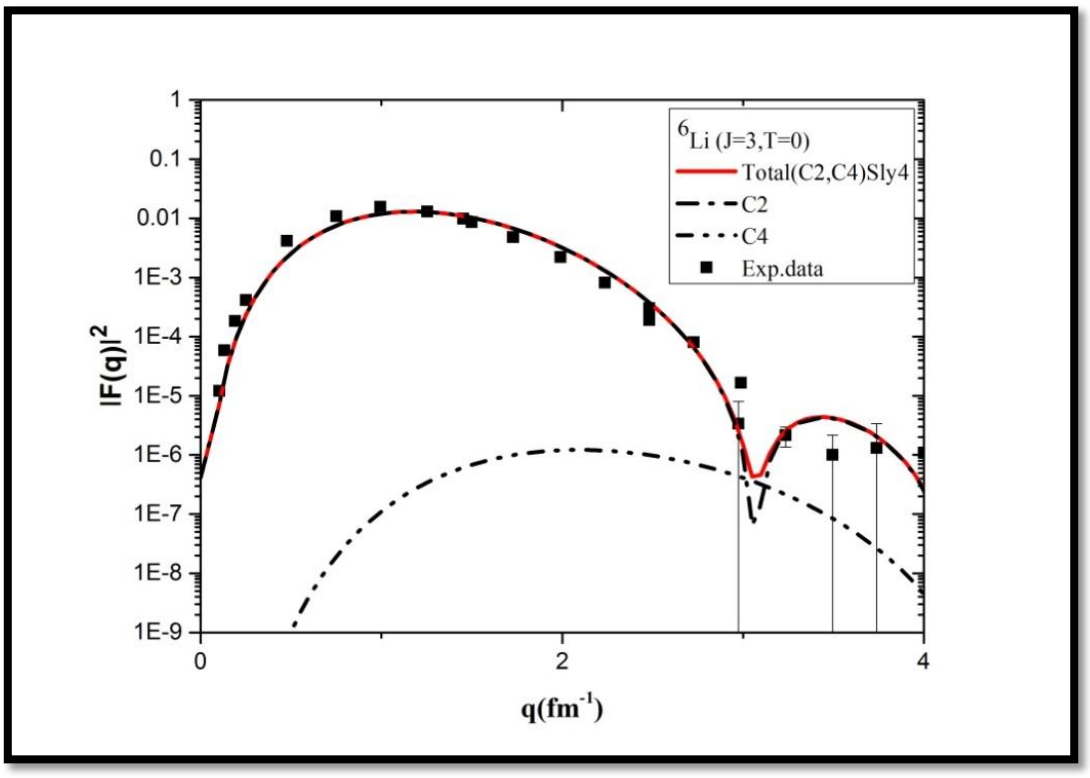

Fig. (3.10): Total longitudinal (C2+C4) inelastic form factor-factor and individual contribution to the $J^{\pi}T = 3^{+}\ 0$(E_x=2.186MeV)state calculated with a Skyrme potential of ^{6}Li. The data are taken from Refs [52,53].

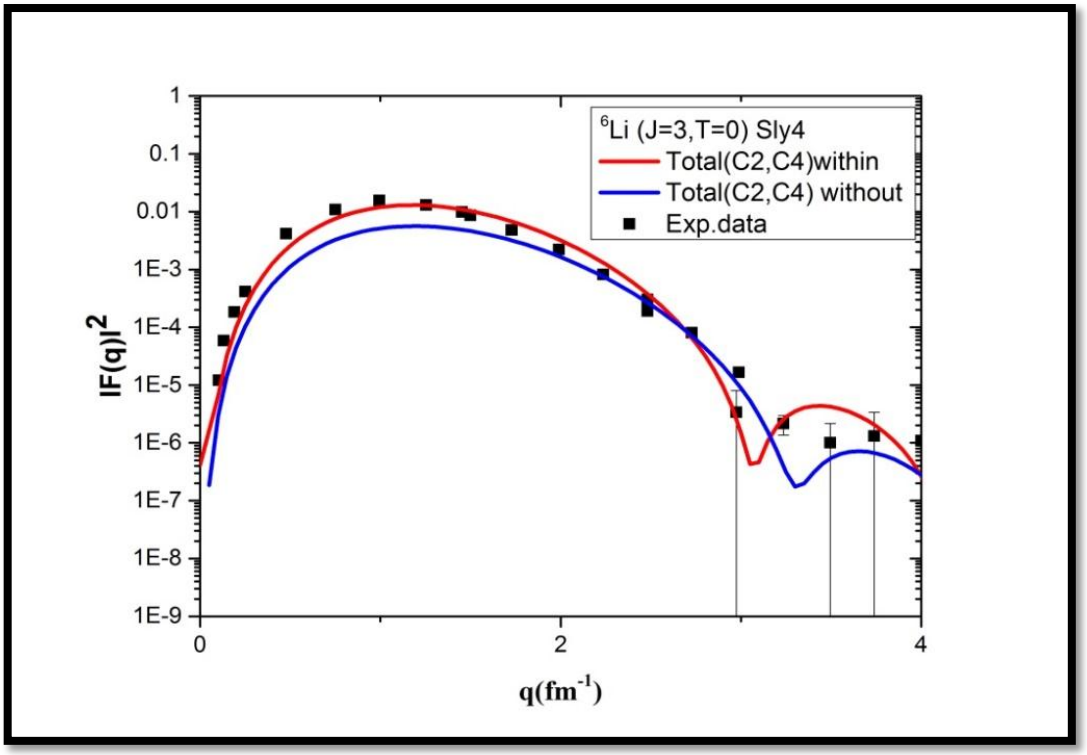

Fig.(3.11): Total (C2+C4) longitudinal elastic form factor for the $J^{\pi}T = 3^{+}\ 0$ (E_x=2.186MeV) state calculated with and without effective charge using Skyrme potential in ^{6}Li. The data are taken from Refs. [52,53]

3.2.4 Transverse Form Factors for (1, 0) state

Figure (3.12) shows purely isoscalar M1 transverse elastic form factors for the $J^{\pi}T = 1^{+}\ 0$ state in ^{6}Li calculated with (0+2)ħω truncated using spsdpf (rad-short dash) and psd (black-short dash) potentials. The calculation form factor with spsdpf model potential describes the experimental data well for the first maximum and after then start to deviate the data and show a decline in value at the second maximum. The calculation form factors with a psd model space fall to reproduce the structure at $q > 1\ fm^{-1}$ and shifting the diffraction minimum to higher momentum. The One-body density matrix element values for this transition M1 is shown in tables (3.5)

Figure (3.13) shows purely isoscalar M1 transverse elastic form factor for the $J^{\pi}T = 1^{+}\ 0$ state in ^{6}Li calculated with (0+2) ħω truncated using Wood-Saxon (rad-short dash) and Skyrme (black-short dash) potentials. The calculation form factor with WS potential describes the experimental data for the first maximum and after then starts to deviate the data and showed a decline in value at the second maximum. The calculation form factors with (0+2) ħω truncated using Skyrme (sly4) potentials fall to reproduce the structure at $0.6 > q > 2.4\ fm^{-1}$. But these calculations reproduce the experimental data at higher momentum transfer $q > 2.4 fm^{-1}$.

Table (3.5): The calculated M1 transition OBDM element values for $J^{\pi}T = 3^{+}\ 0$ (E_x= 2.186 MeV) in ^{6}Li nucleus.

^{6}Li		M1
j_i	j_f	OBDM(ΔT=0)
$1s_{1/2}$	$1s_{1/2}$	3.34355
$1s_{1/2}$	$2s_{1/2}$	0.11360
$1p_{3/2}$	$1p_{3/2}$	0.63887
$1p_{3/2}$	$2p_{3/2}$	0.04354
$1p_{1/2}$	$1p_{1/2}$	0.84030
$1p_{1/2}$	$2p_{1/2}$	0.05047
$1d_{5/2}$	$1d_{5/2}$	0.02176
$1d_{3/2}$	$1d_{3/2}$	0.02597
$2s_{1/2}$	$1s_{1/2}$	0.11360
$2s_{1/2}$	$2s_{1/2}$	0.02479
$1f_{5/2}$	$1f_{5/2}$	0.00042
$2p_{3/2}$	$1p_{3/2}$	0.04354
$2p_{3/2}$	$2p_{3/2}$	0.00359
$2p_{1/2}$	$1p_{1/2}$	0.05047
$2p_{1/2}$	$2p_{1/2}$	0.00380

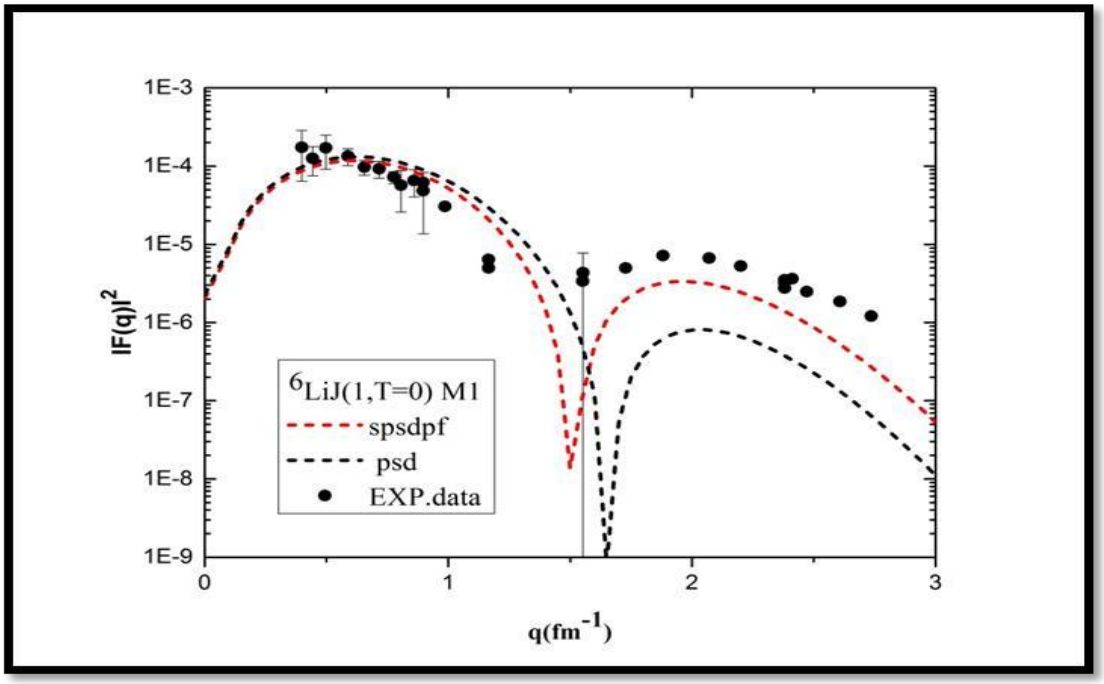

Fig.(3.12): The elastic transverse M1 form factor for the $J^{\pi}T = 1^{+}\ 0$ state in ^{6}Li calculated with spsdpf model space truncation to (0+2)$\hbar\omega$ and psd model space. The data are taken from Ref. [2,52,53].

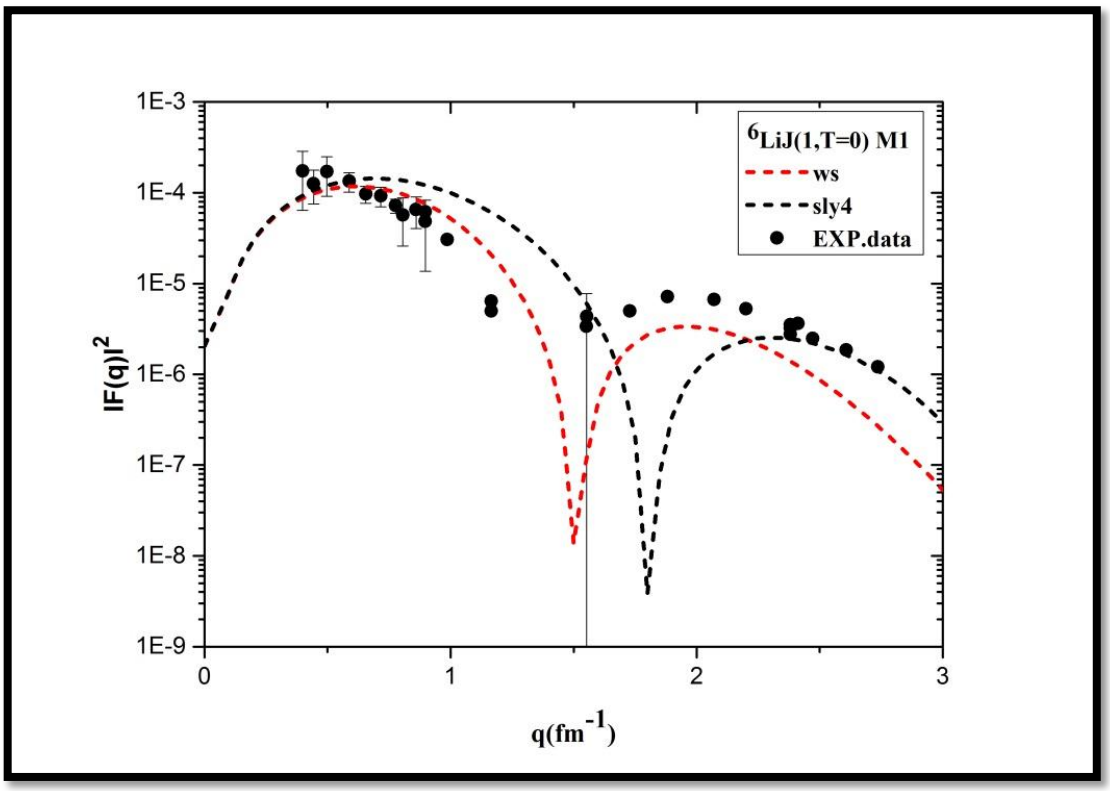

Fig.(3.13): The M1 transverse elastic form factor for the $J^{\pi}T = 1^{+}\ 0$ state in ^{6}Li calculated with (0+2) ħω truncated. The data are taken from Refs. [2,52,53]

3.2.5 Transverse Form Factors for (0, 1) state

The calculation of the pure isovector Ml transition form factor excited from the ground state $J^{\pi}T = 1^{+}\ 0$ to the $J^{\pi}T = 0^{+}\ 1$ state at $E_x = 3.56$ MeV in ^{6}Li is displayed in figure (3.14). The calculation form factor with spsdpf model space (rad-short dash) describes the data better than the spd model space (black-short dash) at $q < 1\ fm^{-1}$. The One-body density matrix element values for this transition M1 is shown in tables (3.6)

The calculation pure isovector Ml transition form factor with both WS and Skyrme potentials are displayed in figure (3.15). The calculation form factor with WS (rad-short dash) and Skyrme (black-short dash) potentials both describes the data very well at $q > 1\ fm^{-1}$ and shows diffraction minimum shifting to higher momentum transfer. After that, the calculation form factor with Skyrme (sly4) potential show an agreement with experimental data at $q > 2.2 fm^{-1}$ while the calculation with WS underestimates the data at $q > 1.7 fm^{-1}$.

Table (3.6): The calculated M1 transition OBDM values for $J^{\pi}T = 0^{+}\ 1$ (E_x= 3.56 MeV) in ^{6}Li nucleus.

^{6}Li		M1
j_i	j_f	OBDM(ΔT=1)
$1s_{1/2}$	$1s_{1/2}$	-0.00813
$1s_{1/2}$	$1d_{3/2}$	-0.01125
$1s_{1/2}$	$2s_{1/2}$	0.01269
$1p_{3/2}$	$1p_{3/2}$	-0.18026
$1p_{3/2}$	$1p_{1/2}$	0.31450
$1p_{3/2}$	$1f_{5/2}$	0.01051
$1p_{3/2}$	$2p_{3/2}$	-0.01799

$1p_{3/2}$	$2p_{1/2}$	**0.02368**
$1p_{1/2}$	$1p_{3/2}$	**-0.38574**
$1p_{1/2}$	$1p_{1/2}$	**-0.18069**
$1p_{1/2}$	$2p_{3/2}$	**-0.02649**
$1p_{1/2}$	$2p_{1/2}$	**-0.00543**
$1d_{5/2}$	$1d_{5/2}$	**-0.00255**
$1d_{5/2}$	$1d_{3/2}$	**0.00493**
$1d_{3/2}$	$1s_{1/2}$	**0.01085**
$1d_{3/2}$	$1d_{5/2}$	**-0.00448**
$1d_{3/2}$	$1d_{3/2}$	**-0.00039**
$1d_{3/2}$	$2s_{1/2}$	**-0.00198**
$2s_{1/2}$	$1s_{1/2}$	**-0.01046**
$2s_{1/2}$	$1d_{3/2}$	**-0.00045**
$2s_{1/2}$	$2s_{1/2}$	**-0.00011**
$2p_{3/2}$	$1p_{3/2}$	**-0.00505**
$2p_{3/2}$	$1p_{1/2}$	**0.00892**
$2p_{3/2}$	$1f_{5/2}$	**0.00031**
$2p_{3/2}$	$2p_{3/2}$	**-0.00054**
$2p_{3/2}$	$2p_{1/2}$	**0.00071**
$2p_{1/2}$	$1p_{3/2}$	**-0.00531**
$2p_{1/2}$	$1p_{1/2}$	**-0.00253**
$2p_{1/2}$	$2p_{3/2}$	**-0.00038**
$2p_{1/2}$	$2P_{1/2}$	**-0.00008**

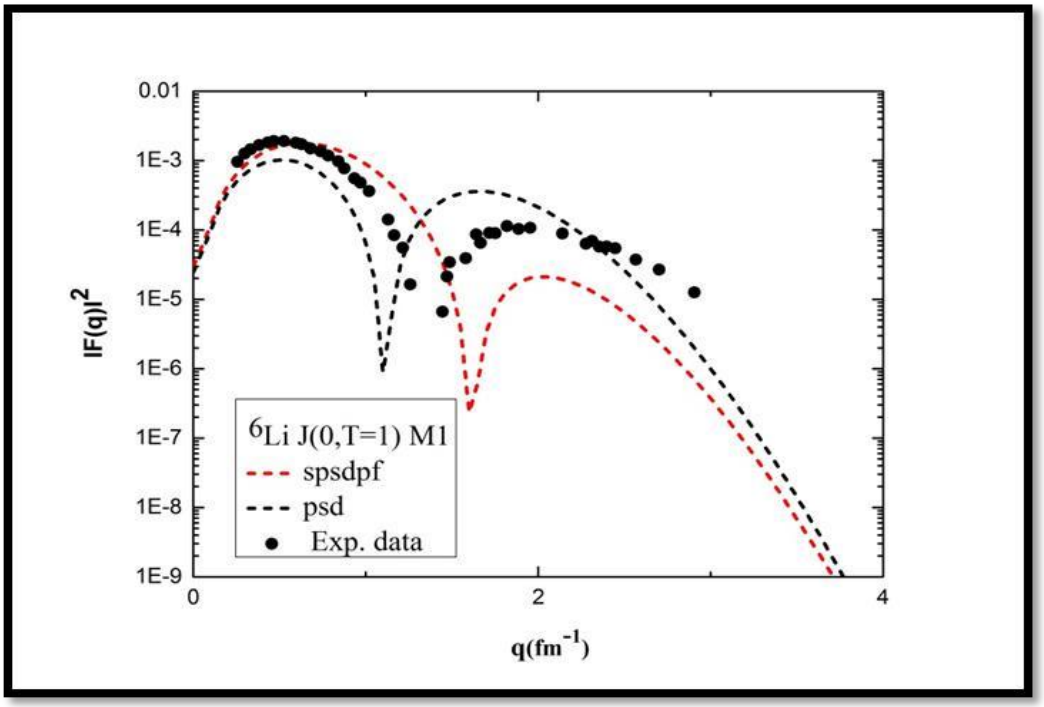

Fig.(3.14) Transverse form factors (M1) for electroexcitation to the $J^{\pi}T = 0^{+}\,1$ (E_x=3.56 MeV) state in ^{6}Li calculated with (0+2) ħω truncated. The data are taken from Refs. [2, 52,53]

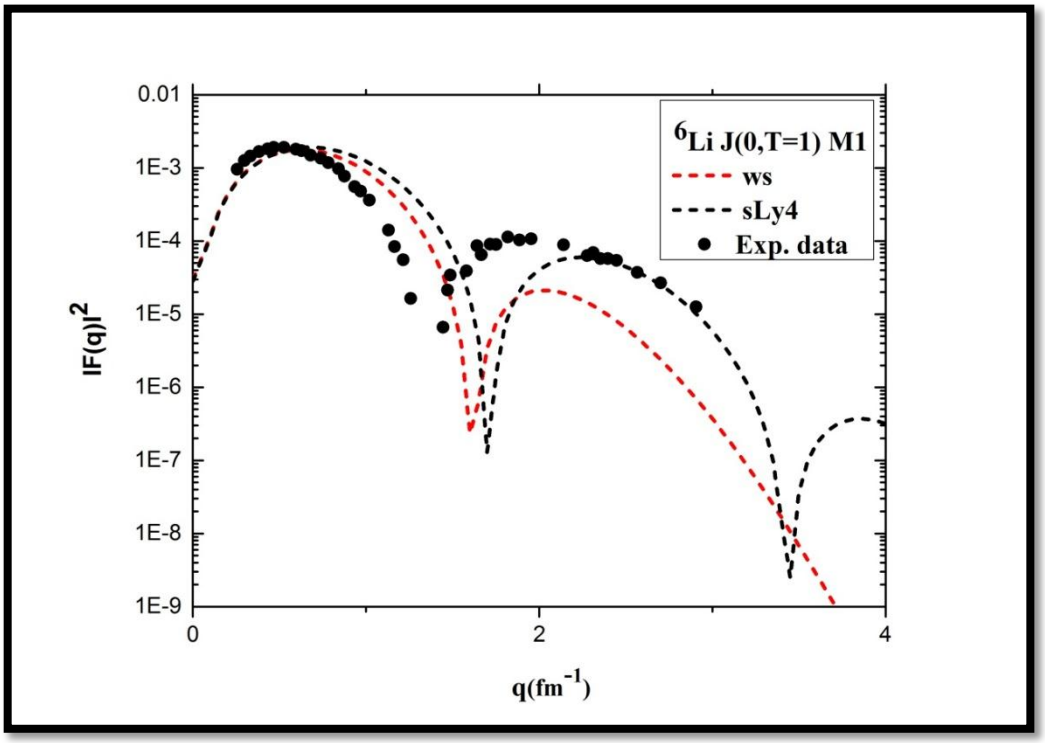

Fig.(3.15): Magnetic M1 transverse form factor for electroexcitation of the $J^{\pi}T = 0^{+}\,1$ (E_x=3.56 MeV) state in ^{6}Li calculated with (0+2) ħω truncated. The data are taken from Refs. [2,52,53]

3.2.6 Transverse Form Factors for (2, 1) state

Figure (3.16) shows the total multipole transition (M1+E2+M3) red solid line and individual form factor using WS potential for the $J^{\pi}T = 2^{+}\ 1$ (5.36) MeV state in ^{6}Li. The calculation result with spsdpf model space depicts the data very well in shape and slightly overestimates the data in magnitude for all momentum transfers. While the calculation results with psd model space describe the experimental data well at $q < 1\ fm^{-1}$ as shown in figure (3.17). The calculation results with Skyrme potential fall to describe the experimental data in shape and magnitude as shows in figure (3.18).

Table (3.7): The calculated M1 transition OBDM values for ($J^{\pi}T = 2^{+}\ 1$) (E_x= 5.36 MeV) in ^{6}Li nucleus.

^{6}Li		M1
j_i	j_f	OBDM(ΔT=1)
$1s_{1/2}$	$1s_{1/2}$	0.01569
$1s_{1/2}$	$1d_{3/2}$	0.02041
$1s_{1/2}$	$2s_{1/2}$	0.02015
$1p_{3/2}$	$1p_{3/2}$	-0.02324
$1p_{3/2}$	$1p_{1/2}$	-0.66110
$1p_{3/2}$	$1f_{5/2}$	-0.00273
$1p_{3/2}$	$2p_{3/2}$	-0.00754
$1p_{3/2}$	$2p_{1/2}$	-0.03791
$1p_{1/2}$	$1p_{3/2}$	0.08426
$1p_{1/2}$	$1p_{1/2}$	0.51526
$1p_{1/2}$	$2p_{3/2}$	0.00941
$1p_{1/2}$	$2p_{1/2}$	0.03918
$1d_{5/2}$	$1d_{5/2}$	-0.00055
$1d_{5/2}$	$1d_{3/2}$	-0.00302
$1d_{3/2}$	$1s_{1/2}$	0.00035
$1d_{3/2}$	$1d_{5/2}$	0.00102
$1d_{3/2}$	$1d_{3/2}$	0.00158
$1d_{3/2}$	$2s_{1/2}$	0.00173

$2s_{1/2}$	$1s_{1/2}$	-0.02322
$2s_{1/2}$	$2s_{1/2}$	-0.00059
$1f_{7/2}$	$1f_{5/2}$	-0.00037
$1f_{5/2}$	$1p_{3/2}$	0.00893
$1f_{5/2}$	$1f_{7/2}$	0.00006
$1f_{5/2}$	$2p_{3/2}$	0.00070
$2p_{3/2}$	$1p_{3/2}$	-0.00010
$2p_{3/2}$	$1p_{1/2}$	0.00547
$2p_{3/2}$	$1f_{5/2}$	0.00002
$2p_{3/2}$	$2p_{3/2}$	0.00004
$2p_{3/2}$	$2p_{1/2}$	0.00032
$2p_{1/2}$	$1p_{3/2}$	-0.00079
$2p_{1/2}$	$1p_{1/2}$	-0.00442
$2p_{1/2}$	$2p_{3/2}$	-0.00008
$2p_{1/2}$	$2p_{1/2}$	-0.00035

Table(3.8): The calculated E2 transition OBDM values for ($J^{\pi}T = 2^{+}\ 1$) (E_x= 5.36 MeV) in ^{6}Li nucleus.

^{6}Li		E2
j_i	j_f	OBDM(ΔT=1)
$1s_{1/2}$	$1d_{5/2}$	0.00307
$1s_{1/2}$	$1d_{3/2}$	-0.00225
$1p_{3/2}$	$1P_{3/2}$	0.12616
$1p_{3/2}$	$1P_{1/2}$	0.12449
$1p_{3/2}$	$1F_{5/2}$	-0.00721
$1p_{3/2}$	$2P_{3/2}$	--0.00309
$1p_{3/2}$	$2P_{1/2}$	0.01821
$1p_{1/2}$	$1p_{3/2}$	0.21845
$1p_{1/2}$	$1f_{5/2}$	0.00348
$1p_{1/2}$	$2p_{3/2}$	0.02187
$1d_{5/2}$	$1s_{1/2}$	0.01519
$1d_{5/2}$	$1d_{5/2}$	0.00056
$1d_{5/2}$	$1d_{3/2}$	0.00267
$1d_{5/2}$	$2s_{1/2}$	-0.00004
$1d_{3/2}$	$1s_{1/2}$	0.01846
$1d_{3/2}$	$1d_{5/2}$	0.00210
$1d_{3/2}$	$1d_{3/2}$	-0.00108
$1d_{3/2}$	$2s_{1/2}$	-0.00021

$2s_{1/2}$	$1d_{5/2}$	**-0.00014**
$2s_{1/2}$	$1d_{3/2}$	**0.00017**
$1f_{7/2}$	$1p_{3/2}$	**0.00459**
$1f_{7/2}$	$1f_{5/2}$	**-0.00029**
$1f_{7/2}$	$2p_{3/2}$	**0.00049**
$1f_{5/2}$	$1p_{3/2}$	**0.00644**
$1f_{5/2}$	$1p_{1/2}$	**-0.00130**
$1f_{5/2}$	$1f_{5/2}$	**0.00009**
$1f_{5/2}$	$2p_{3/2}$	**0.00047**
$1f_{5/2}$	$2p_{1/2}$	**-0.00021**
$2p_{3/2}$	$1p_{3/2}$	**-0.00141**
$2p_{3/2}$	$1p_{1/2}$	**-0.00066**
$2p_{3/2}$	$1f_{5/2}$	**0.00006**
$2p_{3/2}$	$2p_{3/2}$	**-0.00006**
$2p_{3/2}$	$2p_{1/2}$	**-0.00014**
$2p_{1/2}$	$1p_{3/2}$	**-0.00184**
$2p_{1/2}$	$1f_{5/2}$	**-0.00003**
$2p_{1/2}$	$2p_{3/2}$	**-0.00020**

Table (3.9): The calculated M3 transition OBDM values for ($J^{\pi}T = 2^{+}$ 1) (E_x= 5.36 MeV) in ^{6}Li nucleus.

^{6}Li		**M3**
j_i	j_f	**OBDM(ΔT=1)**
$1s_{1/2}$	$1d_{5/2}$	**-0.01584**
$1s_{1/2}$	$1d_{3/2}$	**0.02041**
$1s_{1/2}$	$2s_{1/2}$	**0.02015**
$1p_{3/2}$	$1p_{3/2}$	**-0.02324**
$1p_{3/2}$	$1p_{1/2}$	**-0.66110**
$1p_{3/2}$	$1f_{5/2}$	**-0.00273**
$1p_{3/2}$	$2p_{3/2}$	**-0.00754**
$1p_{3/2}$	$2p_{1/2}$	**-0.03791**
$1p_{1/2}$	$1p_{3/2}$	**0.08426**
$1p_{1/2}$	$1p_{1/2}$	**0.51526**
$1p_{1/2}$	$2p_{3/2}$	**0.00941**
$1p_{1/2}$	$2p_{1/2}$	**0.03918**
$1d_{5/2}$	$1d_{5/2}$	**-0.00055**
$1d_{5/2}$	$1d_{3/2}$	**-0.00302**
$1d_{3/2}$	$1s_{1/2}$	**0.00035**
$1d_{3/2}$	$1d_{5/2}$	**0.00102**

$1d_{3/2}$	$1d_{3/2}$	0.00158
$1d_{3/2}$	$2s_{1/2}$	0.00173
$2s_{1/2}$	$1s_{1/2}$	-0.02322
$2s_{1/2}$	$2s_{1/2}$	-0.00059
$1f_{7/2}$	$1f_{5/2}$	-0.00037
$1f_{5/2}$	$1p_{3/2}$	0.00893
$1f_{5/2}$	$1f_{7/2}$	0.00006
$1f_{5/2}$	$2p_{3/2}$	0.00070
$2p_{3/2}$	$1p_{3/2}$	-0.00010
$2p_{3/2}$	$1p_{1/2}$	0.00547
$2p_{3/2}$	$1f_{5/2}$	0.00002
$2p_{3/2}$	$2p_{3/2}$	0.00004
$2p_{3/2}$	$2p_{1/2}$	0.00032
$2p_{1/2}$	$1p_{3/2}$	-0.00079
$2p_{1/2}$	$1p_{1/2}$	-0.00442
$2p_{1/2}$	$2p_{3/2}$	-0.00008
$2p_{1/2}$	$2p_{1/2}$	-0.00035

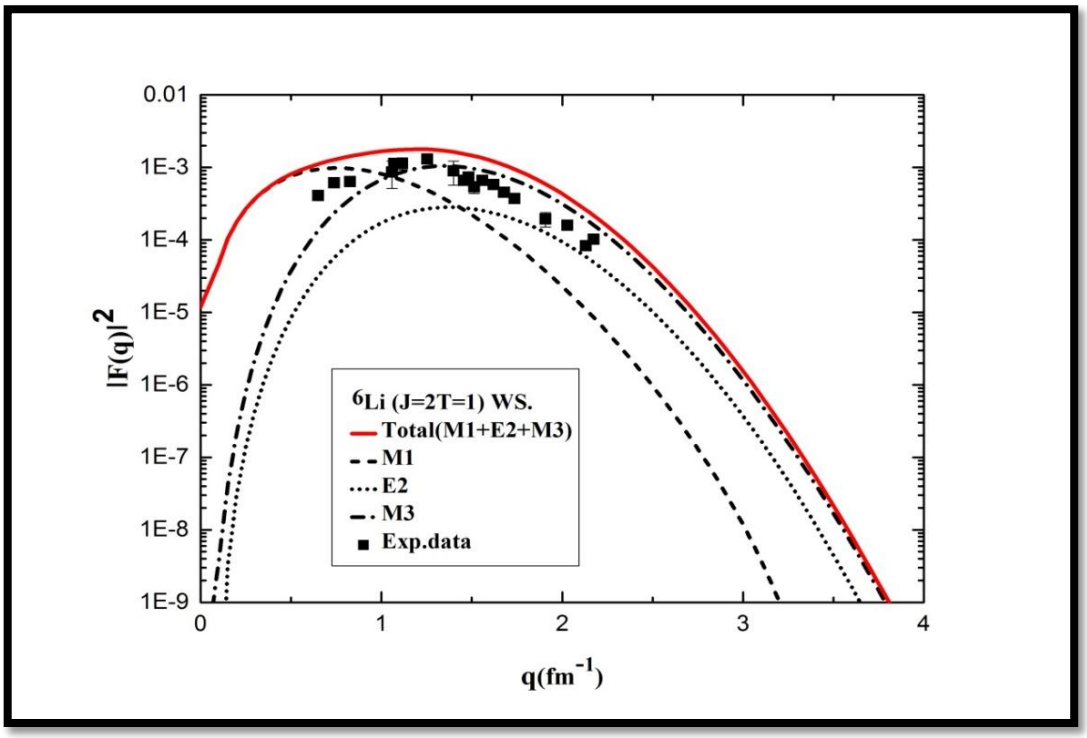

Fig.(3.16): Total (M1+E2+M3) and individual transverse form factor for the $J^{\pi}T = 2^{+}$ 1(E_x= 5.36 MeV) state in ^{6}Li using large basis spsdpf. The data are taken from Refs. [2,52,53]

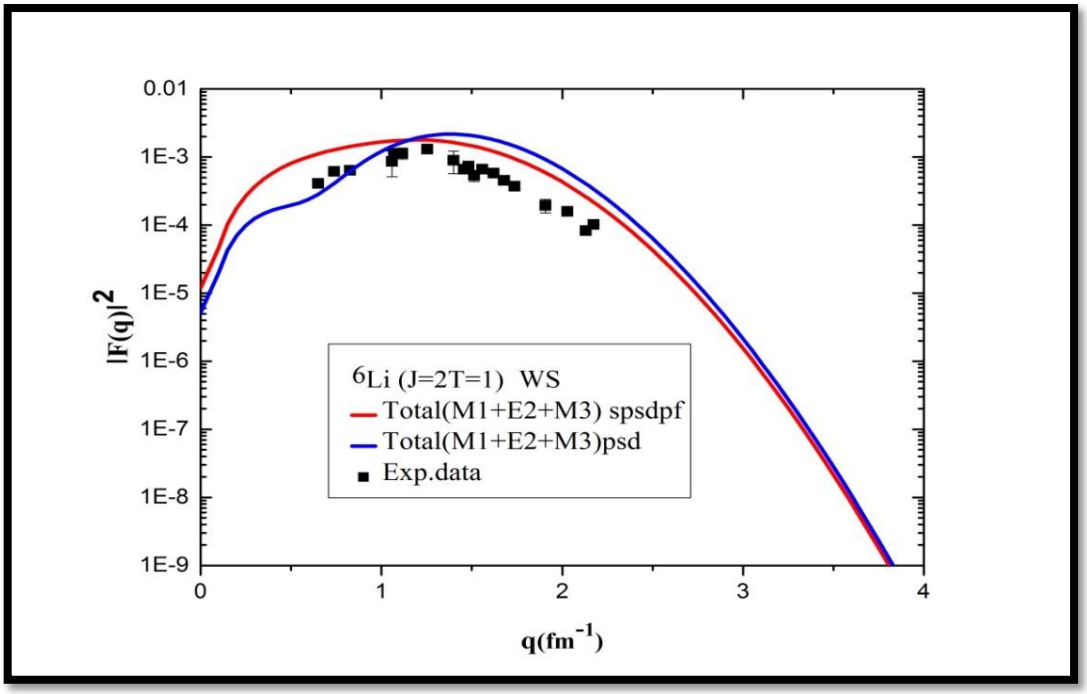

Fig.(3.17): The total (M1+E2+M3) and individual transverse form factor for the $J^{\pi}T = 2^{+}\ 1$(E_x= 5.36 MeV) state in ^{6}Li calculated with (0+2)ħω truncated using Skyrme potential. The data are taken from Refs. [2,52,53]

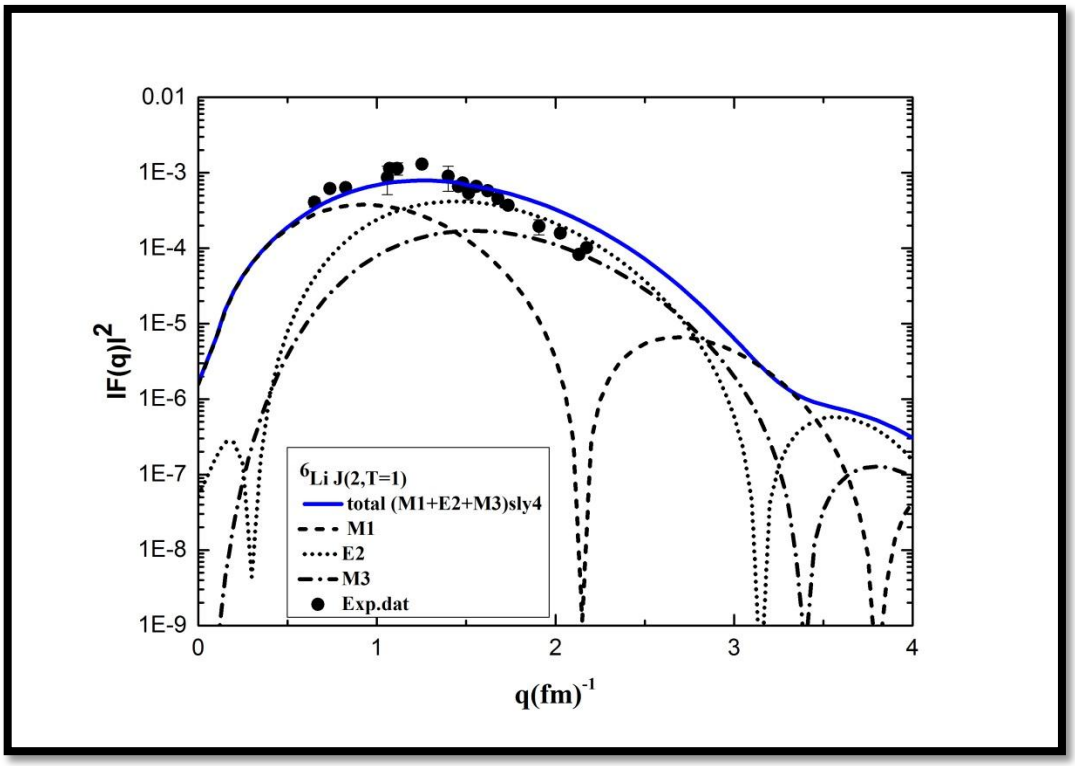

Fig.(3.18) Total transverse (M1+E2+M3) and individual form factor for the $J^{\pi}T = 2^{+}\ 1$ (E_x= 5.36 MeV) state calculated with Skyrme (sly4) potential in ^{6}Li nuclei. The data are taken from Refs. [2,52,53].

3.3 The ^{9}Be nucleus:

The Beryllium has eleventh known isotopes, only the ^{9}Be is stable and primordial nuclide [54]. We present the result obtained for the longitudinal and transverse form factors to understand the general features of the electromagnetic transitions in the most complicated spsdpf-shell nucleus, the even Z and odd N nucleus ^{9}Be.

3.3.1 Energy levels

The calculation energy levels scheme with a large basis spsdpf and psd model-space are displayed in Fig: (3.19). The calculation result of the energy level scheme for the ^{9}Be nucleus with spsdpf model-space truncated to (0+2) ħω using Warburton-Brown interaction shows an acceptable agreement with experimental schemes at the lowest energy band. While the higher band, their calculated value is less than the experimental data within limits of about 1.6-2.8 MeV. The truncation to 2ħω is found sufficient convergence in these states because the truncate to 4 and 6 ħω give only a slight change in energy levels of the higher shell only. Although the psd model-space calculated energy level is in a reasonable agreement with the experimental results at the lowest energy band, while the higher band shows a greater value than the experimental data with about 3-6 MeV.

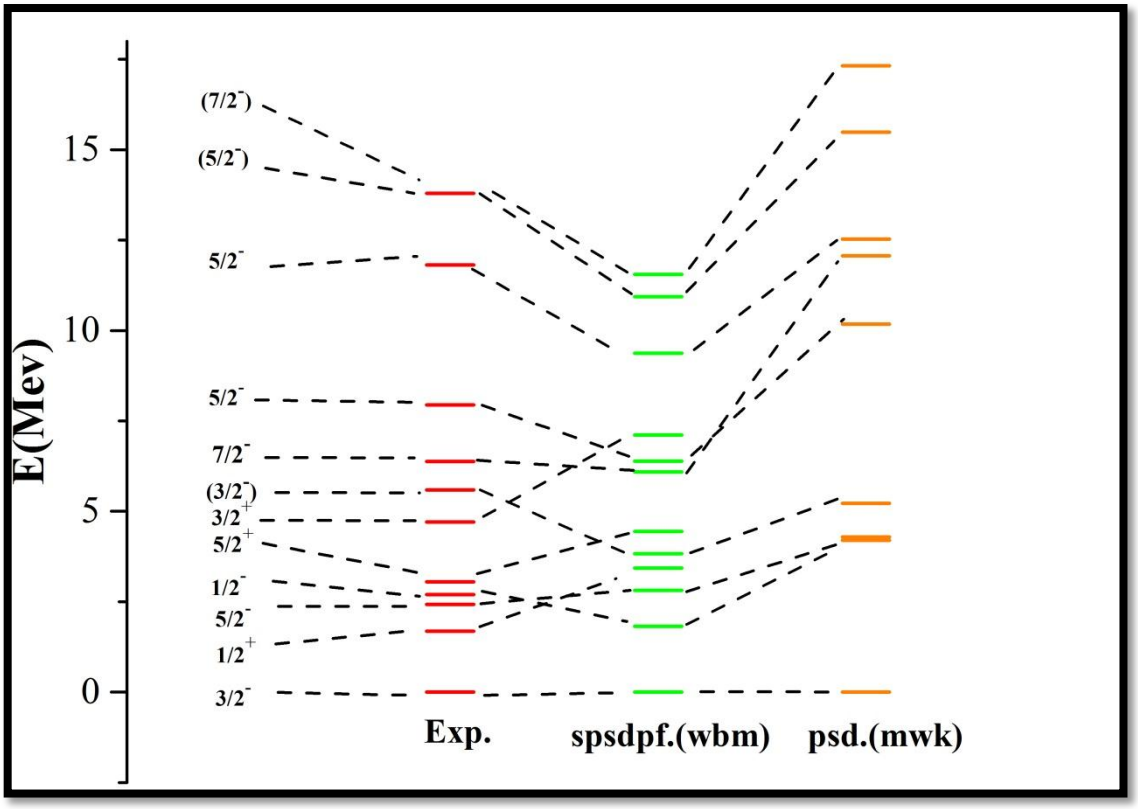

Fig: (3.19): The energy level scheme for the positive and negative parity states of ^{9}Be nucleus compared with data taken from Ref. [55]

3.3.2 The longitudinal form factor for (J=3/2, T=1/2) state

The elastic longitudinal C2 form factor of the ($J^{\pi} = 3/2^{-}, T = 1/2$) in ^{9}Be calculated with the spsdpf-shell truncated to (0+2) hω. All calculation form factors accomplished it in the spsdpf model space with Warburton-Brown interaction. The calculation results of Skyrme potential were compared with the data are taken from Ref. [56]. The One-body density matrix element values for this transition C0 and C2 are shown in tables (3.10), (3.11) respectively.

The total longitudinal (C0+C2) form factor calculated for spsdpf model space with (0+2) ħω truncation and the individual contribution is displayed in figure (3.20). The result calculation of the Skyrme (Sly4) potential without effective charge showed excellent agreement with the

experimental data. Also, Figure (3.20) shows how the C0 and C2 are exchanged to influence all transfer momentum. This indicates that the one body density matrix element has been appropriately chosen.

Table(3.10): The calculated C0 transition OBDM element values for $(J^{\pi}T = 3/2^{-}\ 1/2$ in ^{9}Be nucleus.

^{9}Be		C0	
j_i	j_f	OBDM(ΔT=0)	OBDM(ΔT=1)
$1s_{1/2}$	$1s_{1/2}$	5.65462	0.00012
$1s_{1/2}$	$2s_{1/2}$	-0.03042	-0.00007
$1p_{3/2}$	$1p_{3/2}$	3.69736	0.98776
$1p_{3/2}$	$2P_{3/2}$	0.09207	-0.00934
$1p_{1/2}$	$1p_{1/2}$	1.69068	0.01262
$1p_{1/2}$	$2p_{1/2}$	0.07050	-0.00284
$1d_{5/2}$	$1d_{5/2}$	0.03751	0.00134
$1d_{3/2}$	$1d_{3/2}$	0.03553	0.00092
$2s_{1/2}$	$1s_{1/2}$	-0.03042	-0.00007
$2s_{1/2}$	$2s_{1/2}$	0.02849	0.00021
$1f_{7/2}$	$1f_{7/2}$	0.00003	0.00003
$1f_{5/2}$	$1f_{5/2}$	0.00006	0.00002
$2p_{3/2}$	$1p_{3/2}$	0.09207	-0.00934
$2p_{3/2}$	$2p_{3/2}$	0.00463	0.00053
$2p_{1/2}$	$1p_{1/2}$	0.07050	-0.00284
$2p_{1/2}$	$2p_{1/2}$	0.00332	-0.00012

Table(3.11): The calculated C2 transition OBDM element values for $(J^{\pi}T = 3/2^{-}\ 1/2$ in ^{9}Be nucleus.

^{9}Be		C2	
j_i	j_f	OBDM(ΔT=0)	OBDM(ΔT=1)
$1s_{1/2}$	$1d_{5/2}$	0.00738	0.00361
$1s_{1/2}$	$1d_{3/2}$	0.00410	0.00069
$1p_{3/2}$	$1p_{3/2}$	-0.38767	0.30236
$1p_{3/2}$	$1p_{1/2}$	-0.43376	0.14527

$1p_{3/2}$	$1f_{7/2}$	-0.00182	-0.00147
$1p_{3/2}$	$1f_{5/2}$	-0.00062	-0.00095
$1p_{3/2}$	$2p_{3/2}$	-0.04229	-0.01962
$1p_{3/2}$	$2p_{1/2}$	-0.02121	0.00338
$1p_{1/2}$	$1p_{3/2}$	0.43376	-0.14527
$1p_{1/2}$	$1f_{5/2}$	-0.00085	0.00027
$1p_{1/2}$	$2p_{3/2}$	0.01715	-0.00264
$1d_{5/2}$	$1s_{1/2}$	0.00738	0.00361
$1d_{5/2}$	$1d_{5/2}$	-0.00349	0.00057
$1d_{5/2}$	$1d_{3/2}$	-0.00319	-0.00020
$1d_{5/2}$	$2s_{1/2}$	-0.00282	-0.00064
$1d_{3/2}$	$1s_{1/2}$	-0.00410	-0.00069
$1d_{3/2}$	$1d_{5/2}$	0.00319	0.00020
$1d_{3/2}$	$1d_{3/2}$	-0.00434	-0.00052
$1d_{3/2}$	$2s_{1/2}$	0.00282	-0.00010
$2s_{1/2}$	$1d_{5/2}$	-0.00282	-0.00064
$2s_{1/2}$	$1d_{3/2}$	-0.00282	0.00010
$1f_{7/2}$	$1p_{3/2}$	-0.00182	-0.00147
$1f_{7/2}$	$1f_{7/2}$	0.00000	0.00001
$1f_{7/2}$	$2p_{3/2}$	-0.00003	-0.00002
$1f_{5/2}$	$1p_{3/2}$	0.00062	0.00095
$1f_{5/2}$	$1p_{1/2}$	-0.00085	0.00027
$1f_{5/2}$	$2p_{3/2}$	0.00003	0.00003
$1f_{5/2}$	$2p_{1/2}$	-0.00002	0.00002
$2p_{3/2}$	$1p_{3/2}$	-0.04229	-0.01962
$2p_{3/2}$	$1p_{1/2}$	-0.01715	0.00264
$2p_{3/2}$	$1f_{7/2}$	-0.00003	-0.00002
$2p_{3/2}$	$1f_{5/2}$	-0.00003	-0.00003
$2p_{3/2}$	$2p_{3/2}$	-0.00050	0.00026
$2p_{3/2}$	$2p_{1/2}$	-0.00079	0.00006
$2p_{1/2}$	$1p_{3/2}$	0.02121	-0.00338
$2p_{1/2}$	$2p_{1/2}$	-0.00002	0.00002
$2p_{1/2}$	$2p_{3/2}$	0.00079	-0.00006

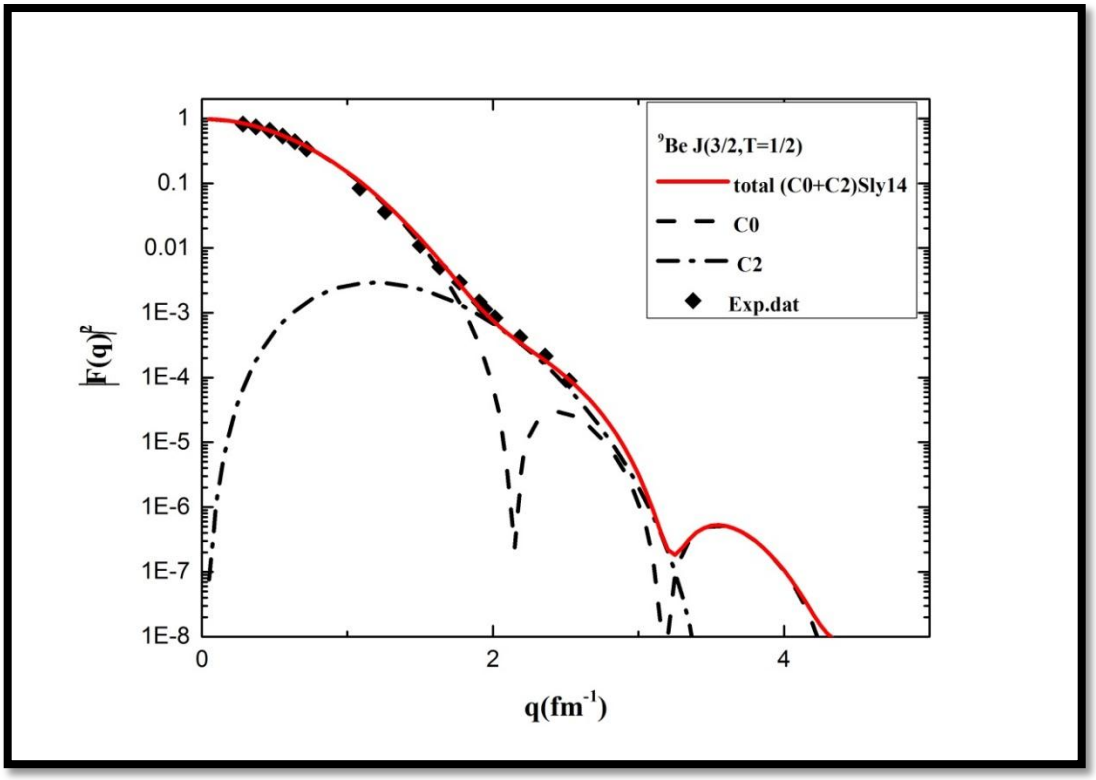

Fig (3.20): Total Longitudinal (C0+C2) elastic form factors and individual multipole for the $J^{\pi}T = 3/2^{-}\ 1/2$ state in ^{9}Be calculated with the spsdpf-shell truncated to (0+2) ħω. The data are taken from refs. [56].

3.3.3 The longitudinal form factor for (5/2, 1/2)state

The C2 Longitudinal form factors transition from the ground state $(J^{\pi} = 3/2^{-},\ T = 1/2)$ to the $(J^{\pi} = 5/2^{-},\ T = 1/2)$ state at E_x=2.43MeV are calculated and the result compared with the data are taken from [56]. The One-body density matrix (OBDM) element values for this transition C2 are shown in tables (3.12).

The calculation results without effective charge underestimate the experimental data at all momentum transfer and shift the diffraction minimum to higher momentum as shown in figure (3.21).

Figure (3.22) shown the large-basis calculation form factors truncated to (0 + 2)hω using WS (black -short dash) and Skyrme (red-short dash) potentials. The Skyrme (sly4) calculation with bare effective charge (2.2, 0.8) agrees well with the experimental data for all transfer momentum and shows a diffraction minimum at $q = 2.8\, fm^{-1}$. While the calculation with WS overestimates the data at $q > 2 fm^{-1}$ and shifts a diffraction minimum to higher momentum transfer at about $q \approx 2.4\, fm^{-1}$.

Table(3.12): The calculated C2 transition OBDM element values for $(J^{\pi}T = 5/2^{-}\ 1/2)$ in ^{9}Be nucleus.

^{9}Be		**C2**	
j_i	j_f	**OBDM(ΔT=0)**	**OBDM(ΔT=1)**
$1s_{1/2}$	$1d_{5/2}$	**-0.01191**	**-0.00156**
$1s_{1/2}$	$1d_{3/2}$	**-0.00988**	**-0.00189**
$1p_{3/2}$	$1p_{3/2}$	**0.70350**	**-0.45829**
$1p_{3/2}$	$1p_{1/2}$	**1.17762**	**0.14101**
$1p_{3/2}$	$1f_{7/2}$	**0.00227**	**0.00112**
$1p_{3/2}$	$1f_{5/2}$	**0.00097**	**-0.00030**
$1p_{3/2}$	$2p_{3/2}$	**0.03453**	**-0.00758**
$1p_{3/2}$	$2p_{1/2}$	**0.04531**	**-0.00007**
$1p_{1/2}$	$1p_{3/2}$	**-1.25988**	**-0.25894**
$1p_{1/2}$	$1f_{5/2}$	**0.00147**	**0.00060**
$1p_{1/2}$	$2p_{3/2}$	**-0.03997**	**-0.00446**
$1d_{5/2}$	$1s_{1/2}$	**-0.01093**	**-0.00532**
$1d_{5/2}$	$1d_{5/2}$	**0.01051**	**0.00135**
$1d_{5/2}$	$1d_{3/2}$	**0.00465**	**0.00028**
$1d_{5/2}$	$2s_{1/2}$	**0.00634**	**0.00051**
$1d_{3/2}$	$1s_{1/2}$	**0.00756**	**0.00120**
$1d_{3/2}$	$1d_{5/2}$	**-0.00339**	**0.00023**
$1d_{3/2}$	$1d_{3/2}$	**0.00885**	**0.00041**
$1d_{3/2}$	$2s_{1/2}$	**-0.00321**	**0.00041**
$2s_{1/2}$	$1d_{5/2}$	**0.00432**	**-0.00003**
$2s_{1/2}$	$1d_{3/2}$	**0.00596**	**-0.00079**
$1f_{7/2}$	$1P_{3/2}$	**0.00364**	**0.00276**

$1f_{7/2}$	$1f_{7/2}$	0.00001	0.00001
$1f_{7/2}$	$1f_{5/2}$	0.00001	0.00001
$1f_{7/2}$	$2p_{3/2}$	0.00009	0.00004
$1f_{5/2}$	$1p_{3/2}$	0.00053	0.00166
$1f_{5/2}$	$1p_{1/2}$	0.00272	0.00090
$1f_{5/2}$	$2p_{3/2}$	-0.00006	-0.00004
$1f_{5/2}$	$2p_{1/2}$	0.00010	0.00002
$2p_{3/2}$	$1p_{3/2}$	0.03710	0.00217
$2p_{3/2}$	$1p_{1/2}$	0.02622	-0.00375
$2p_{3/2}$	$1f_{7/2}$	0.00009	0.00002
$2p_{3/2}$	$1f_{5/2}$	0.00002	-0.00003
$2p_{3/2}$	$2p_{3/2}$	0.00135	0.00004
$2p_{3/2}$	$2p_{1/2}$	0.00127	-0.00010
$2p_{1/2}$	$1p_{3/2}$	-0.03784	0.00170
$2p_{1/2}$	$1f_{5/2}$	0.00007	0.00002
$2p_{1/2}$	$2p_{3/2}$	-0.00144	-0.00001

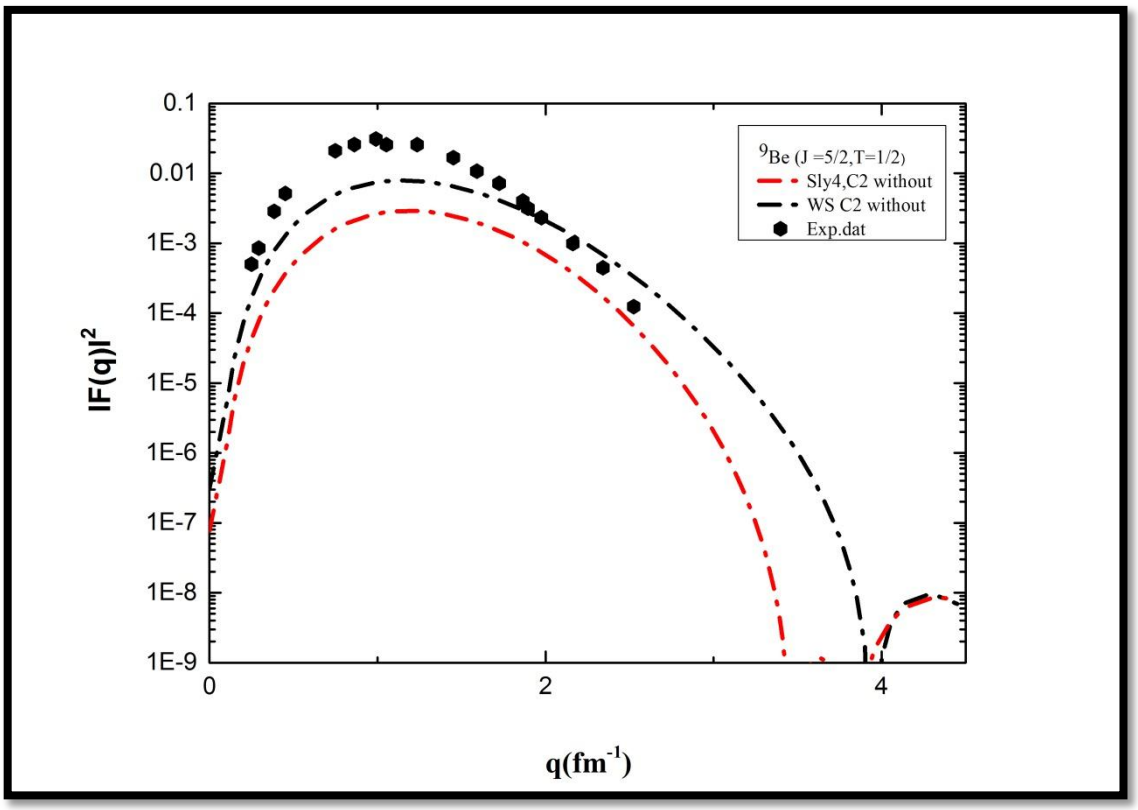

Fig. (3.21): The C2 Longitudinal inelastic form factor of $J^{\pi}T = 5/2^{-}\ 1/2$ (E_x=2.43 MeV) state in ^{9}Be nucleus. The large basis spsdpf truncated to (0+2) ħω calculation without effective charge using Skyrme and Ws potential. The data are from refs. [56].

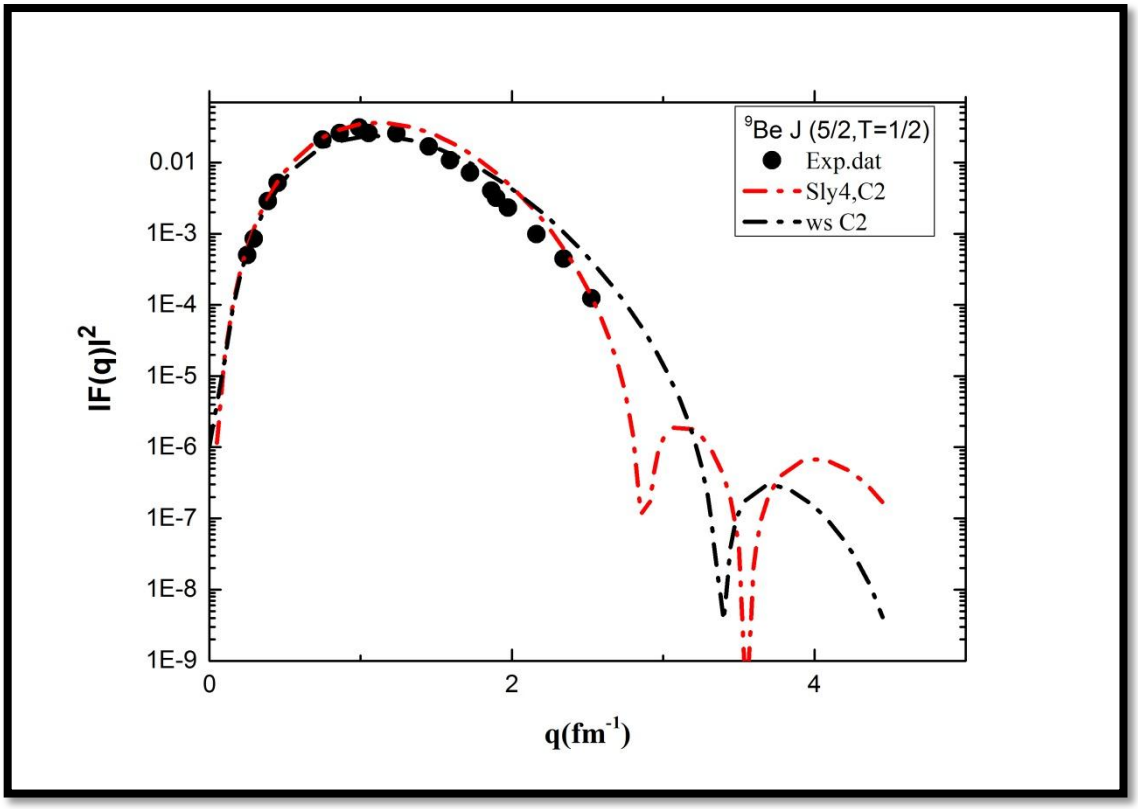

Fig. (3.22): The C2 Longitudinal inelastic form factor of $J^{\pi}T = 5\backslash 2^{-}\ 1\backslash 2$ (E_x=2.43 MeV) state in ^{9}Be nucleus. The large basis spsdpf truncated to (0+2) ħω calculation with effective charge using Skyrme and Ws potential. The data are from refs. [56].

3.3.4 The longitudinal form factor for (7/2,1/2)state

The C2 Longitudinal transition form factors from the ground state ($J^{\pi} = 3/2^{-},\ T = 1/2$) to the (($J^{\pi} = 7/2^{-},\ T = 1/2$) state at E_x= 6.38 MeV are calculated and the result compared with the data are taken from [58]. The One-body density matrix (OBDM) element values for the C2 transition is shown in tables (3.13)

The calculation result without effective charge is poorly reproduced in both potentials. The form factor is underestimated the experimental data at momentum transfer data $q \leq 1.5 fm^{-1}$ and overestimate slightly the

experimental data at momentum transfer $q \geq 1.8 fm^{-1}$ as shown in figure (3.23).

Figure (3.24) shows the large-basis calculation form factors truncated to (0+2) hω with bare effective charge (0.8, 0.4). The WS (black dash-dot) and Skyrme (sly4) (red dash-dot) potentials calculations agree well with the experimental data for $q = 1.5\, fm^{-1}$and after then started to overestimate the experimental data gradually. The Skyrme calculations show a slight improvement in convergence from the experimental data at higher transfer momentum.

Table (3.13): The calculated C2 transition OBDM element values for $(J^{\pi}T = 7/2^{-}\ 1/2)$ in ^{9}Be nucleus.

^{9}Be		**C2**	
j_i	j_f	**OBDM(ΔT=0)**	**OBDM(ΔT=1)**
$1s_{1/2}$	$1d_{5/2}$	**0.01126**	**0.00057**
$1s_{1/2}$	$1d_{3/2}$	**0.00952**	**0.00008**
$1p_{3/2}$	$1p_{3/2}$	**-0.68224**	**0.37394**
$1p_{3/2}$	$1p_{1/2}$	**-0.40512**	**0.22360**
$1p_{3/2}$	$1f_{7/2}$	**-0.00118**	**-0.00086**
$1p_{3/2}$	$1f_{5/2}$	**-0.00036**	**-0.00129**
$1p_{3/2}$	$2p_{3/2}$	**-0.03497**	**0.00838**
$1p_{3/2}$	$2p_{1/2}$	**-0.02791**	**0.00357**
$1P_{1/2}$	$1p_{3/2}$	**0.68528**	**0.01019**
$1p_{1/2}$	$1f_{5/2}$	**-0.00162**	**-0.00098**
$1p_{1/2}$	$2p_{3/2}$	**0.02950**	**0.00237**
$1d_{5/2}$	$1s_{1/2}$	**0.00606**	**0.00785**
$1d_{5/2}$	$1d_{5/2}$	**-0.00547**	**-0.00042**
$1d_{5/2}$	$1d_{3/2}$	**-0.00218**	**0.00031**
$1d_{5/2}$	$2s_{1/2}$	**-0.00156**	**0.00233**
$1d_{3/2}$	$1s_{1/2}$	**-0.00110**	**-0.00037**
$1d_{3/2}$	$1d_{5/2}$	**0.00283**	**-0.00005**
$1d_{3/2}$	$1d_{3/2}$	**-0.00546**	**-0.00019**
$1d_{3/2}$	$2s_{1/2}$	**0.00383**	**-0.00023**
$2s_{1/2}$	$1d_{5/2}$	**-0.00263**	**-0.00042**
$2s_{1/2}$	$1d_{3/2}$	**-0.00321**	**-0.00042**
$1f_{7/2}$	$1p_{3/2}$	**-0.00633**	**-0.00678**

$1f_{7/2}$	$1f_{7/2}$	-0.00001	-0.00001
$1f_{7/2}$	$1f_{5/2}$	0.00000	-0.00001
$1f_{7/2}$	$2p_{3/2}$	0.00020	0.00018
$1f_{5/2}$	$1p_{3/2}$	0.00237	0.00165
$1f_{5/2}$	$1p_{1/2}$	0.00028	-0.00003
$1f_{5/2}$	$1f_{5/2}$	-0.00001	0.00000
$1f_{5/2}$	$2p_{3/2}$	0.00009	0.00006
$1f_{5/2}$	$2p_{3/2}$	0.00000	0.00001
$2p_{3/2}$	$1p_{3/2}$	-0.04150	-0.00582
$2p_{3/2}$	$1p_{1/2}$	-0.03370	-0.00856
$2p_{3/2}$	$1f_{7/2}$	-0.00004	-0.00002
$2p_{3/2}$	$1f_{5/2}$	-0.00004	-0.00005
$2p_{3/2}$	$2p_{3/2}$	-0.00144	0.00008
$2p_{3/2}$	$2p_{1/2}$	-0.00136	-0.00006
$2p_{1/2}$	$1p_{3/2}$	0.02050	-0.00186
$2p_{1/2}$	$1f_{5/2}$	-0.00006	-0.00003
$2p_{1/2}$	$2p_{3/2}$	0.00090	-0.00003

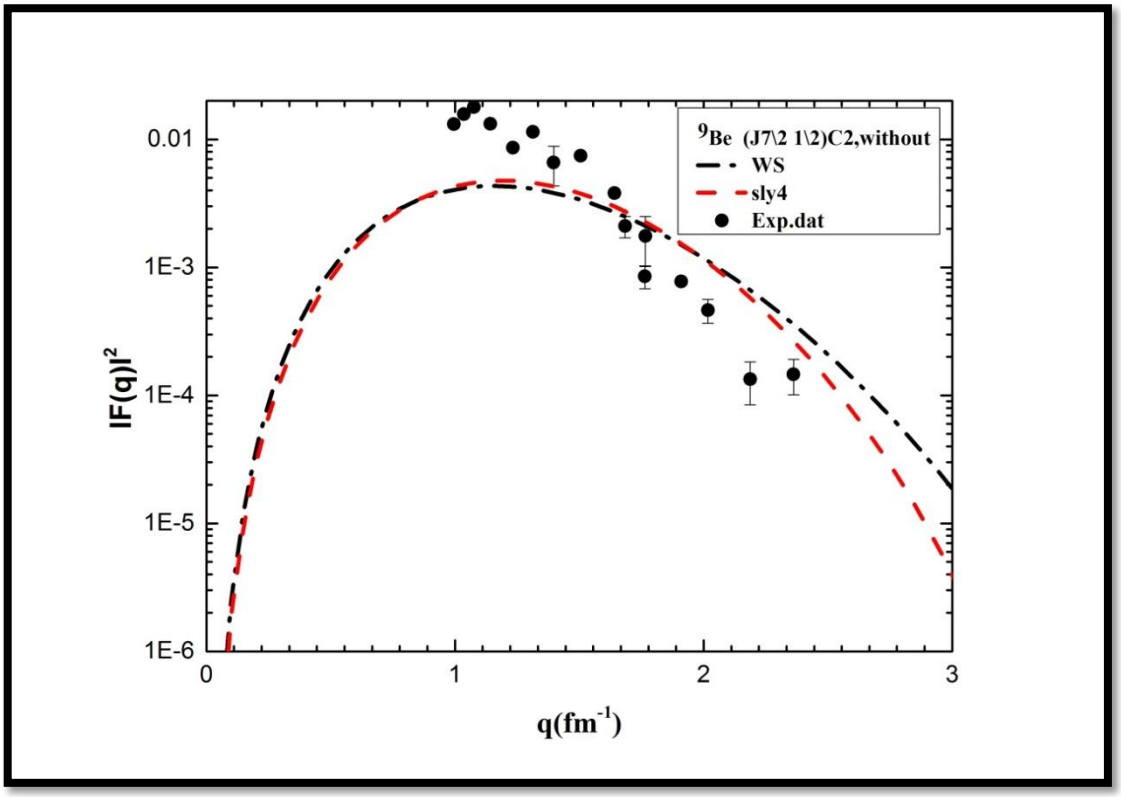

Fig.(3.23): The C2 inelastic longitudinal form factor of the $(J^{\pi} = 7/2, T = 1/2)$ E_x=6.38MeV state in ^{9}Be calculated with the spsdpf-shell with truncated to (0 + 2) $\hbar\omega$. The data are taken from Refs. [56].

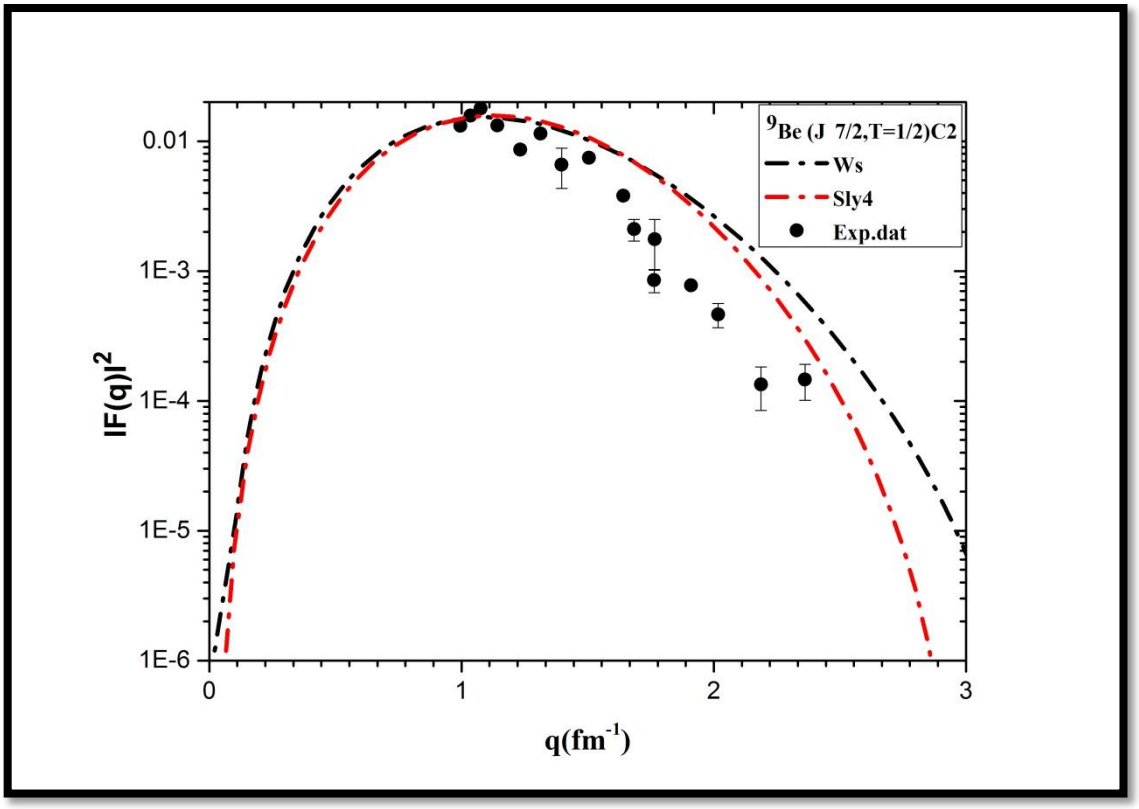

Fig.(3.24): The C2 inelastic longitudinal form factor for the $(J^{\pi} = 7/2, T = 1/2)$ E_x=6.38MeV state in ^{9}Be calculated with the spsdpf-shell with truncated to (0 + 2) $\hbar\omega$. The data are taken from Refs. [56].

3.3.5 Transverse Form Factors for(3/2, 1/2) state

The calculation of the total transverse (M1+M3) form factor for the transition $(J^{\pi}T = 3/2^{-}\ 1/2)$ state in ^{9}Be was done with and without effective charge. The calculation and results compared with the data are taken from [56]. The One-body density matrix element values for this transition M1, M3 are shown in tables (3.14) and (3.15).

Figure (3.25) shows the large-basis calculation using Wood-Saxon potential truncated to (0+2) ħω. The total (M1+M3) red line and the individual contribution M1 (black dash) and M3 (black dot-dot) calculation form factors agree well in shape and slightly overestimate the experimental data in magnitude.

The large-basis calculation truncated to $(0 + 2)\ \hbar\omega$ using Skyrme (sly4) potential shown in figure (3.26) also agreed well in shape and slightly overestimates the experimental data in magnitude.

Table(3.14): The calculated M1 transition OBDM element values for $(J^{\pi}T = 3/2^{-}\ 1/2)$ in ^{9}Be nucleus.

^{9}Be		**M1**	
j_i	j_f	**OBDM(ΔT=0)**	**OBDM(ΔT=1)**
$1s_{1/2}$	$1s_{1/2}$	**0.00002**	**0.00011**
$1s_{1/2}$	$1d_{3/2}$	**0.00183**	**0.00188**
$1s_{1/2}$	$2s_{1/2}$	**0.00127**	**0.00017**
$1p_{3/2}$	$1p_{3/2}$	**0.97720**	**0.64057**
$1p_{3/2}$	$1p_{1/2}$	**0.02908**	**-0.13058**
$1p_{3/2}$	$1f_{5/2}$	**-0.00158**	**-0.00030**
$1p_{3/2}$	$2p_{3/2}$	**-0.00433**	**-0.01688**
$1p_{3/2}$	$2p_{1/2}$	**0.00571**	**0.00132**
$1p_{1/2}$	$1p_{3/2}$	**-0.02908**	**0.13058**
$1p_{1/2}$	$1p_{1/2}$	**0.05069**	**-0.07449**
$1p_{1/2}$	$2p_{3/2}$	**-0.00269**	**-0.00196**
$1p_{1/2}$	$2p_{1/2}$	**0.00213**	**-0.00172**
$1d_{5/2}$	$1d_{5/2}$	**0.00229**	**0.00201**
$1d_{5/2}$	$1d_{3/2}$	**0.00035**	**0.00008**
$1d_{3/2}$	$1s_{1/2}$	**-0.00183**	**-0.00188**
$1d_{3/2}$	$1d_{5/2}$	**-0.00035**	**-0.00008**
$1d_{3/2}$	$1d_{3/2}$	**0.00120**	**0.00043**
$1d_{3/2}$	$2s_{1/2}$	**0.00055**	**-0.00037**
$2s_{1/2}$	$1s_{1/2}$	**0.00127**	**0.00017**
$2s_{1/2}$	$1d_{3/2}$	**-0.00055**	**0.00037**
$2s_{1/2}$	$2s_{1/2}$	**0.00152**	**-0.00035**
$1f_{7/2}$	$1f_{7/2}$	**0.00002**	**0.00002**
$1f_{5/2}$	$1p_{3/2}$	**0.00158**	**0.00030**
$1f_{5/2}$	$1f_{5/2}$	**0.00001**	**0.00000**
$1f_{5/2}$	$2p_{3/2}$	**0.00006**	**-0.00001**
$2p_{3/2}$	$1p_{3/2}$	**-0.00433**	**-0.01688**
$2p_{3/2}$	$1p_{1/2}$	**0.00269**	**0.00196**
$2p_{3/2}$	$1f_{5/2}$	**-0.00006**	**0.00001**
$2p_{3/2}$	$2p_{3/2}$	**0.00071**	**0.00016**
$2p_{3/2}$	$2p_{1/2}$	**0.00015**	**0.00022**
$2p_{1/2}$	$1p_{3/2}$	**-0.00571**	**-0.00132**

$2p_{1/2}$	$1p_{1/2}$	0.00213	-0.00172
$2p_{1/2}$	$2p_{3/2}$	-0.00015	-0.00022
$2p_{1/2}$	$2p_{1/2}$	0.00005	-0.00010

Table(3.15): The calculated M3 transition OBDM element values for $(J^{\pi}T = 3/2^{-}\ 1/2)$ in ^{9}Be nucleus.

^{9}Be		M3	
j_i	j_f	OBDM(ΔT=1)	OBDM(ΔT=1)
$1s_{1/2}$	$1d_{5/2}$	0.00244	0.00280
$1p_{3/2}$	$1p_{3/2}$	0.79829	0.78361
$1p_{3/2}$	$1f_{7/2}$	-0.00301	-0.00246
$1p_{3/2}$	$1f_{5/2}$	0.00033	0.00092
$1p_{3/2}$	$2p_{3/2}$	-0.01142	-0.00965
$1p_{1/2}$	$1f_{7/2}$	-0.00062	-0.00076
$1p_{1/2}$	$1f_{5/2}$	-0.00028	0.00007
$1d_{5/2}$	$1s_{1/2}$	0.00244	0.00280
$1d_{5/2}$	$1d_{5/2}$	-0.00140	0.00035
$1d_{5/2}$	$1d_{3/2}$	0.00098	-0.00035
$1d_{5/2}$	$2s_{1/2}$	-0.00006	-0.00036
$1d_{3/2}$	$1d_{5/2}$	-0.00098	0.00035
$1d_{3/2}$	$1d_{3/2}$	0.00021	0.00013
$2s_{1/2}$	$1d_{5/2}$	-0.00006	-0.00036
$1f_{7/2}$	$1p_{3/2}$	-0.00301	-0.00246
$1f_{7/2}$	$1p_{1/2}$	0.00062	0.00076
$1f_{7/2}$	$1f_{7/2}$	0.00001	0.00001
$1f_{7/2}$	$1f_{5/2}$	-0.00001	0.00000
$1f_{7/2}$	$2p_{3/2}$	-0.00007	-0.00005
$1f_{5/2}$	$1p_{3/2}$	-0.00033	-0.00092
$1f_{5/2}$	$1p_{1/2}$	-0.00028	0.00007
$1f_{5/2}$	$1f_{7/2}$	0.00001	0.00000
$1f_{5/2}$	$1f_{5/2}$	0.00000	-0.00001
$1f_{5/2}$	$2p_{3/2}$	0.00000	-0.00003
$1f_{5/2}$	$2p_{1/2}$	0.00000	-0.00001
$2p_{3/2}$	$1p_{3/2}$	-0.01142	-0.00965
$2p_{3/2}$	$1f_{7/2}$	-0.00007	-0.00005
$2p_{3/2}$	$1f_{5/2}$	0.00000	0.00003
$2p_{3/2}$	$2p_{3/2}$	0.00037	0.00057
$2p_{3/2}$	$1f_{5/2}$	0.0000	-0.00001

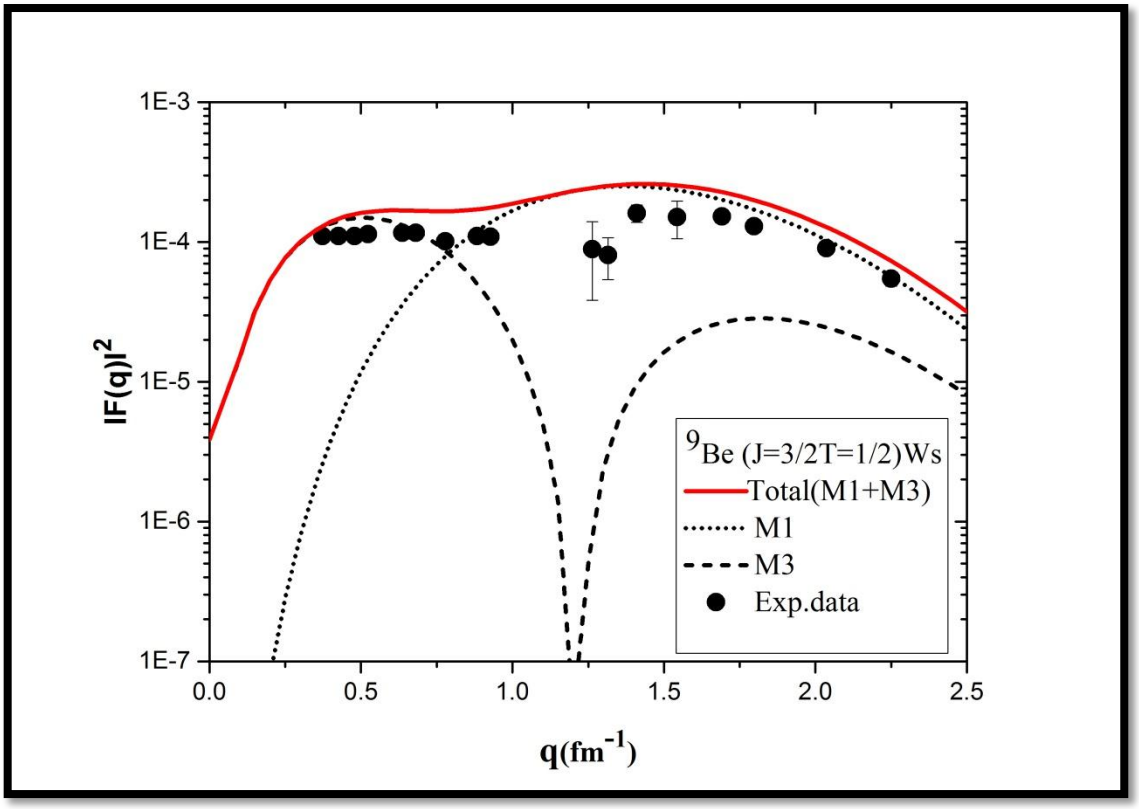

Fig.(3.25): Total transverse (M1+M3) inelastic form factor for the $J^{\pi} = 3/2,\ T = 1/2$ state in ^{9}Be calculated using WS potential with the spsdpf model-space truncated to (0 + 2) $\hbar\omega$. The data are taken from refs. [56].

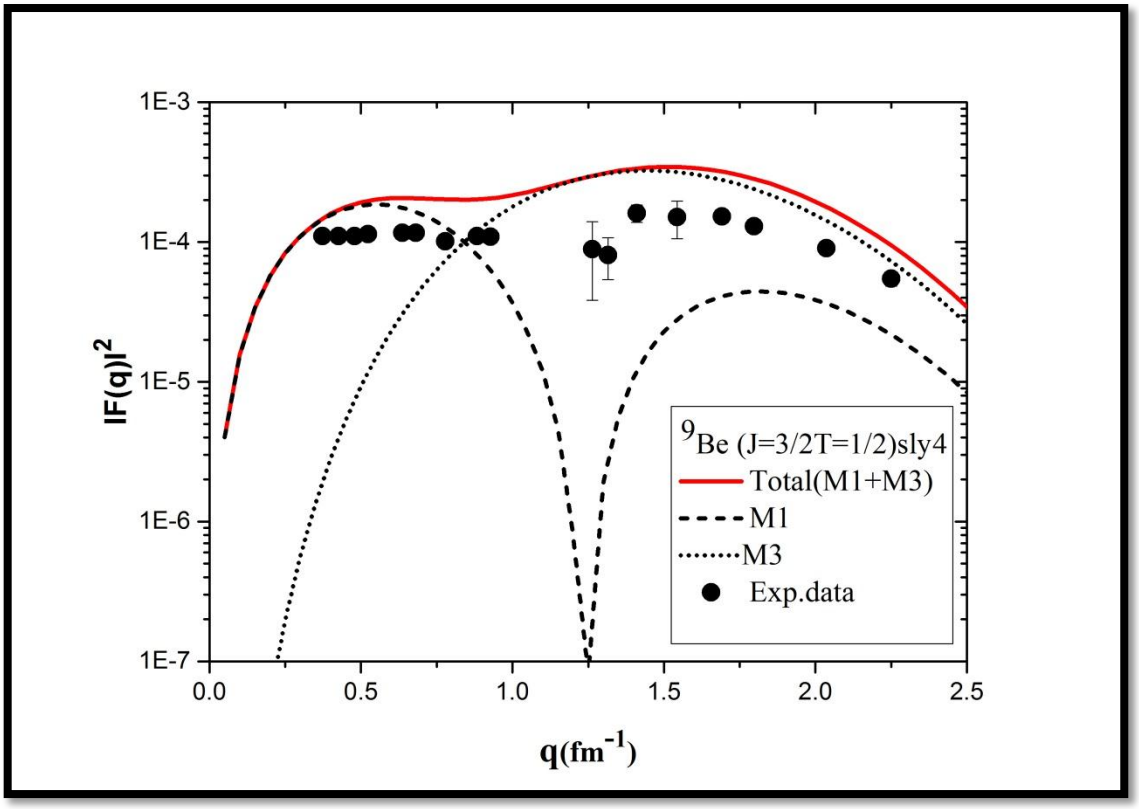

Fig.(3.26): Total transverse (M1+M3) inelastic form factor for the $J^{\pi} = 3/2,\ T = 1/2$ state in ^{9}Be calculated using Skyrme (sly4) potential with the spsdpf model-space truncated to (0 + 2) $\hbar\omega$. The data are taken from refs. [56].

3.3.6 Transverse Form Factors for (5/2, 1/2) state

The calculation of the total transverse (M1+M3) form factor for the $J^{\pi}T = 5/2^{-}\ 1/2$ (E_x=2.43 MeV) state in ^{9}Be and individual contribution display in figure (3.27). The total M1+M3 (red line) and the M1 (black dash) and M3 (black dot-dot) calculation results compared with the data are taken from [56]. The One-body density matrix element values for this transition M1and M3 are shown in tables (3.16) and (3.17).

The large-basis calculation form factor truncated to (0 + 2)hω using WS potential agrees well with the experimental data.

Table (3.16): The calculated M1 transition OBDM element values for $(J^{\pi}T = 5/2^{-}\ 1/2)$ in ^{9}Be nucleus.

^{9}Be		M1	
j_i	j_f	OBDM(ΔT=0)	OBDM(ΔT=1)
$1s_{1/2}$	$1s_{1/2}$	-0.00003	0.00000
$1s_{1/2}$	$1d_{3/2}$	-0.00202	-0.00037
$1s_{1/2}$	$2s_{1/2}$	-0.00055	0.00059
$1p_{3/2}$	$1p_{3/2}$	-0.04808	-0.56579
$1p_{3/2}$	$1p_{1/2}$	-0.14250	-0.36062
$1p_{3/2}$	$1f_{5/2}$	0.00064	-0.00046
$1p_{3/2}$	$2p_{3/2}$	0.00585	-0.00804
$1p_{3/2}$	$2p_{1/2}$	0.00048	-0.00910
$1p_{1/2}$	$1p_{3/2}$	-0.33750	-0.10233
$1p_{1/2}$	$1p_{1/2}$	0.14051	-0.15687
$1p_{1/2}$	$2p_{3/2}$	-0.00762	0.00027
$1p_{1/2}$	$2p_{1/2}$	0.00876	-0.00158
$1d_{5/2}$	$1d_{5/2}$	0.00105	0.00284
$1d_{5/2}$	$1d_{3/2}$	0.00174	0.00001
$1d_{3/2}$	$1s_{1/2}$	0.00315	0.00442
$1d_{3/2}$	$1d_{5/2}$	0.00145	-0.00035
$1d_{3/2}$	$1d_{3/2}$	0.00108	0.00169
$1d_{3/2}$	$2s_{1/2}$	-0.00140	0.00034
$2s_{1/2}$	$1s_{1/2}$	-0.00116	-0.00025
$2s_{1/2}$	$1d_{3/2}$	0.00043	-0.00086
$2s_{1/2}$	$2s_{1/2}$	0.00032	-0.00008
$1f_{7/2}$	$1f_{7/2}$	0.00001	0.00001
$1f_{5/2}$	$1p_{3/2}$	0.00048	0.00042
$1f_{5/2}$	$1f_{5/2}$	-0.00001	-0.00001
$1f_{5/2}$	$2p_{3/2}$	0.00000	0.00001
$2p_{3/2}$	$1p_{3/2}$	-0.00004	-0.00003
$2p_{3/2}$	$1p_{1/2}$	0.01750	0.00920
$2p_{3/2}$	$1f_{5/2}$	0.00593	0.00046
$2p_{3/2}$	$2p_{3/2}$	0.00002	-0.00002
$2p_{3/2}$	$2p_{1/2}$	0.00039	0.00024
$2p_{1/2}$	$1p_{3/2}$	0.00017	-0.00009

$2p_{1/2}$	$1p_{1/2}$	-0.00592	0.00162
$2p_{1/2}$	$2p_{3/2}$	0.01042	0.00233
$2p_{1/2}$	$2p_{1/2}$	-0.00017	0.00011

Table(3.17): The calculated M3 transition OBDM element values for $(J^{\pi}T = 5/2^{-}\ 1/2)$ in ^{9}Be nucleus.

^{9}Be		M3	
j_i	j_f	OBDM(ΔT=0)	OBDM(ΔT=1)
$1s_{1/2}$	$1d_{5/2}$	-0.00222	-0.00302
$1p_{3/2}$	$1p_{3/2}$	0.23485	0.27126
$1p_{3/2}$	$1f_{7/2}$	0.00061	0.00106
$1p_{3/2}$	$1f_{5/2}$	-0.00039	0.00044
$1p_{3/2}$	$2p_{3/2}$	0.00198	-0.00019
$1p_{1/2}$	$1f_{7/2}$	0.00081	0.00047
$1p_{1/2}$	$1f_{5/2}$	0.00101	0.00087
$1d_{5/2}$	$1s_{1/2}$	-0.00262	-0.00291
$1d_{5/2}$	$1d_{5/2}$	-0.00032	0.00112
$1d_{5/2}$	$1d_{3/2}$	-0.00065	-0.00007
$1d_{5/2}$	$2s_{1/2}$	0.00153	-0.00013
$1d_{3/2}$	$1d_{5/2}$	0.00021	0.00080
$1d_{3/2}$	$1d_{3/2}$	-0.00055	-0.00015
$2s_{1/2}$	$1d_{5/2}$	0.00102	-0.00069
$1f_{7/2}$	$1p_{3/2}$	0.00089	0.00111
$1f_{7/2}$	$1p_{1/2}$	-0.00162	-0.00094
$1f_{7/2}$	$1f_{7/2}$	0.00002	0.00002
$1f_{7/2}$	$1f_{5/2}$	0.00001	0.00001
$1f_{7/2}$	$2p_{3/2}$	-0.00004	0.00000
$1f_{5/2}$	$1p_{3/2}$	0.00326	0.00192
$1f_{5/2}$	$1p_{1/2}$	0.00060	-0.00012
$1f_{5/2}$	$1f_{7/2}$	0.00001	0.00001
$1f_{5/2}$	$1f_{5/2}$	0.00001	0.00000
$1f_{5/2}$	$2p_{3/2}$	0.00001	-0.00004
$1f_{5/2}$	$2p_{1/2}$	0.00003	0.00001
$2p_{3/2}$	$1p_{3/2}$	-0.00841	-0.00908
$2p_{3/2}$	$1f_{7/2}$	-0.00007	-0.00005
$2p_{3/2}$	$1f_{5/2}$	-0.00004	-0.00001
$2p_{3/2}$	$2p_{3/2}$	-0.00016	-0.00031
$2p_{1/2}$	$1f_{7/2}$	0.00001	0.00000
$2p_{1/2}$	$1f_{5/2}$	0.00003	0.00003

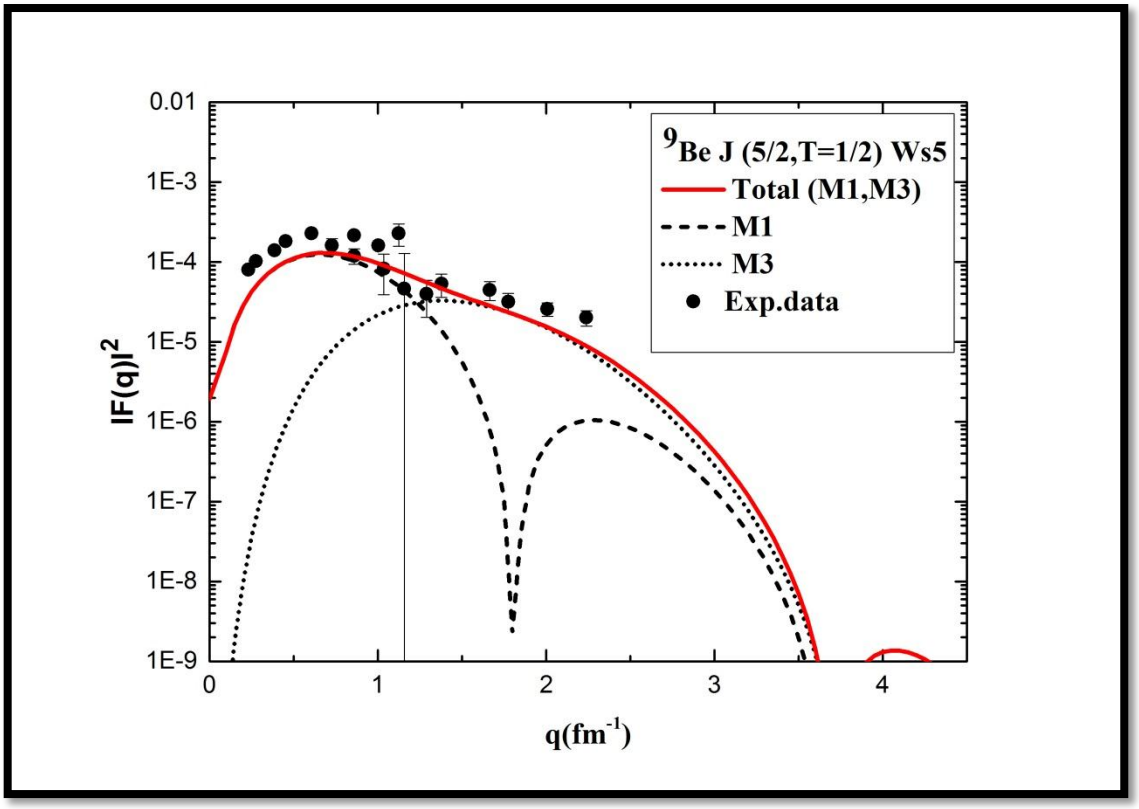

Fig.(3.27): Total transverse (M1+M3) inelastic form factor for the $J^{\pi} = 5/2,\ T = 1/2$ (E_x=2.43 MeV) state in ^{9}Be calculated using WS potential with the spsdpf model-space truncated to (0 + 2) $\hbar\omega$. The data are taken from refs. [56].

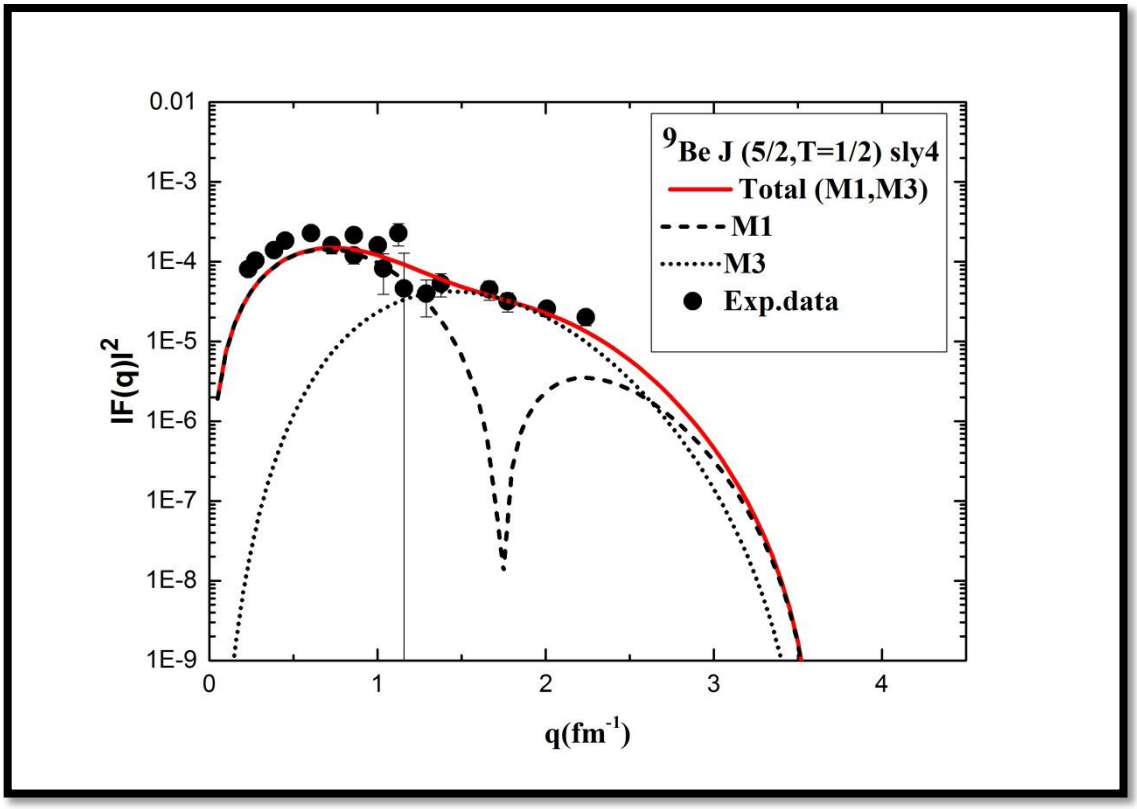

Fig.(3.28): Total transverse (M1+M3) inelastic form factor for the $J^{\pi} = 5/2,\ T = 1/2$ (E_x=2.43 MeV) state in ^{9}Be calculated using Skyrme (sly4) potential with the spsdpf model-space truncated to (0 + 2) $\hbar\omega$. The data are taken from refs. [56].

conclusions

We will briefly summarize the main conclusions of the calculations presented in this work.

1- The calculation results of the elastic and inelastic electron scattering form factor for some p-shell nuclei using large bases with truncation (0+2)ħω agree well with the experimental data.

2- The calculation result with spsdpf model-space truncated to (0+2) $\hbar\omega$ using Warburton-Brown interaction indicates an acceptable agreement with experimental schemes (positive parity levels). Also the truncation to 2 ħω is found to be a sufficient convergence in these states.

3- The calculated form factors for the low excitation state of both nuclei using a Skyrme voltage (sly4) which shows good agreement with experimental data compared to Wood-Saxon.

Future Work

1-Expanding the work presented in this thesis to be applied to the form factors of nuclear states in some nuclei of the sd- shell.

2- Conducting work on other nuclei while using another potential in the framework of the board space used inthis thesis.

References

References

[1] Mohammadi , Saeed, B. N. Giv, and N. S. Shakib. nuclear. Sciences p.1,4 (2017).

[2] Ali .K. Hasan and Azhar.N.Rahim, International Journal of Scientific and Research Publications, p 9, 169 (2018).

[3] Dean, D., et al., Progress in Particle and Nuclear Physics,p.419-500(2004).

[4] Adie D. Salman, Ph.D., Thesis,University of Basrah (2005).

[5] Adie D. Salman, Nadia M. Adeeb Samah, and Oudah Al-Ramahi, Transactions on Engineering and Sciences, p.2347-1964 , (2016).

[6] Deforest, Jr. and J. D. Waleaka, Advance in physics, p.15, 57, 1, (1966).

[7] Jansen, R. Th. Peerdeman and C. devries, Nuclear Physics p. 337-352(1972).

[8] Radhi, Ph.D.thesis, Michigan State University (1983).

[9] Lombard, P. Kossany and G. R. Bishop, Nuclear Physics,p.**59**, 398 (1964).

[10] Cohen and D. Kurath , Nuclear physics ,p.73, 1, (1965).

[11] Adie D. Salman, Samah A. Al-Ramahi, and M. H. Oleiwi, AIP Conference Proceedings p. 2144, 030029 (2019).

[12] Noor Thaer Tilab, Ph.D.Thesis, Usssssss33rniversity of Kerbala (2017).

[13] Glickman, W. Bertozzi, T. N. Buti, S. Dixit, F. W. Hersman, C. E. Hyde-Wright,M. V. Hynes, R. W. Lourie, and B. E. Norum Physical Review C 43, (1991).

[14] Booten, J. and A. Van Hees, Magnetic electron scattering from p-shell nuclei. Nuclear physics p. 510-522(1994).

[15] Kukulin, V.T. Voronchev, T.D. Kaipov, and R.A. Eramzhyan, Nuclear physics. p. 517, 221 (1990).

[16] Karataglidis, B. A. Brown, K. Amos and P. J. Dortmans, Physical Review, p. 2826(1997).

[17] Zeina Abbass Salman , M.Sc., Thesis ,University of Baghdad (2003).

[18] Adie Dawood Salman, Ph.D., Thesis,University of Basrah (2005).

[19] Laith Salih Kadhim Alsalami , M.Sc.,Thesis, University of Baghdad (2006).

[20] Khalid Salih Jassim Al-Jumaili, Ph.D., Thesis, University of Baghdad (2007).

[21] Radhi Z.A. Dakhil, and N.S. Manie, Eur. Phys. J., A50, 115 (2014).

[22]Radhi, Ali A. Alzubadi and Eman M.Rashed, Nuclear Physics p.947,12–25(2016).

[23] Radhi, Ali A. Alzubadi, and A. H. Ali ,Physical Review, p.064312 (2018).

[24] Ali A. Alzubadi, R. A. Radhi, and Noori S. Manie, Physical Review,p. 024316 (2018).

[25] Noor T. Tilab, Adie D. Salman, Journal University of Kerbala , p 15 Scientific (2017).

[26] Wiringa, R. and R. Schiavilla, Microscopic Calculation of ^{6}Li Elastic and Transition Form Factors. Physical Review letters, 81(20): p. 4317(2018).

[27] Radhi, R. and A.A. Alzubadi, Few-Body Systems, p. 1-13 (2019).

[28] Millener, D. I. Sober, H. Crannell, J. T. O'Brien, L. W. Fagg, S. Kowalski, C. F. Williamson, and L. Lapikás Physical Review, p.14(1989).

[29] Lombard, P. Kossany and G. R. Bishop, Nuclear Physics, p. 59, 398 (1964).

[30] Pierre Marmier and E. Sheldon, "Physics of Nuclei and Particle ". Acadmic Press, London, (1969).

[31] Sober, L. W. Fagg, B. Zeidman, R. D. Lawson, D. F. Geesaman, G. C. Morrison, O. Karban, X. K. Maruyama, H. de Vries, E. A. J. M. Offermann, C. W. de Jager, R. A. Lindgren, and J. F. A. van Hienen; Physical Review ,C38,p. 654 (1988).
[32] Adeeb, Journal of Physical Science and Application, **2**,p.392 (2012).

[33] Radhi, Ali A. Alzubadi and Eman M.Rashed, Nuclear Physics, A947,p.12-25 (2016).

[34] bruised and P. W. M. Glademans; "Shell-model Application in Nuclear Spectroscopy", North-Holland Publishing Company, Amsterdam (1977).

[35] Karataglidis, P. Halse and K. Amos, Physical Review, p.2494 (1995).

[36] Henry, A. Kuhnert, J. A. Becker, M. J. Brinkman, T. F. Wang, J. A. Cizewski, W. Korten, F. Azaiez, M. A. Deleplanque, R. M. Diamond, J. E. Draper, W. H. Kelly, A. O. Macchiavelli, and F. S. Stephens, Physical Review., C49, 2849 (1994)

[37] Adie D. Salman and D. R. Kadhim, International Journal of Modern Physics E, 23, 1450054 (2014).
[38] Glickman, W. Bertozzi, T. N. Buti, S. Dixit, F. W. Hersman,C. E.Hyde-Wright, M.V. Hynes, R. W. Lourie, and B. E. Norum, J. J.Kelly, B. L. Berman and D. J. Millener, Physical Review, p. 4 (1991).

[39] Donnelly and J.D. Walecka, Nuclear Physics,p. 81 (1973).

[40] Radhi and E. A. Salman, Nuclear Physics., A 806,179 (2008).
[41] Brown, R. Radhi and B.H. Wildenthal, Physical Review 101,314-358 (1983).
[42] Radhil and A. Bouchebak, Nuclear Physics. A716 .87 (2003).
[43] Thomas, Nature 107, 514 (1926); Frenkel, Zeits. fur Physical 37, 243 (1926).
[44] Vautherin and D. M. Brink, Physical Review, p. 3 (1972).
[45] Skyrme, Nuclear physics p.615-634, (1959).
[46] Vautherin and D. M. Brink, Physics Letters p.149-153.2566(1970).
[47] Warburton, E. and B.A. Brown, Effective interactions for the 0p1s0d nuclear shell-model space. Physical Review C, 46(3): p. 923(1992).

[48] Van Hees, A. and P. Glaudemans, Normal-and nonnormal-parity states in p-shell nuclei. Nuclear Physics A, 396: p. 105-114(1983).
[49] Alex. Brown, Nuclear Physics., A704, 11c, (2002).
[50] Donnelly, W.Haxton, Atomic Data and Nuclear Data Tables, 25, 1, 1, (1980).
[51] Chabanat, P. Bonche, P. Haensel, J. Meyer, R. Schaeffer, Nuclear Physics A635,231-256635 (1998).
[52] Wiringa R. and R. Schiavilla, Physical Review p4317- 4320 (1998).
[53] Dekker, H., Physics Reports, 80(1): p. 1-110. (1981).
[54] Ensslin, Bertozzi, S. Kowalski, C. P. Sargent,. Turchinetz, and C. F. Williamson, Physical Review, (1974).
[55] Jansen, R. Th.Peerdeman and C. DevriesE, Nuclear Physics ,p.337-352, (1972).
[56] Kelly, B. L. Herman and D. J. Millener, Physical Review, (1991).

الخلاصة

تم تطبيق نموذج التوسعة بدون لب مهمل في نوى ^{6}Li و ^{9}Be ، لدراسة التركيب النوي وبعض الخصائص الكهرومغناطيسية لهذه النوى. تضمن حساب نموذج القشرة نوعين من النماذج psd و spsdpf مع تفاعلات psdmwk و wbm على التوالي.

وفقًا لفضاء الانموذج psd و spsdpf ، تم حساب عناصر مصفوفة الكثافة للجسم المنفرد واستخدامه للتحقق من عوامل الشكل المرنة وغير المرنة ومستويات الطاقة للحالة المثارة الواطئة لهذه النوى. اعتمدت دالة الموجة أحادية الابعاد للجسيم المنفرد جهدي وود- سكسن وسكايرم (Sly4).

يكون مستوى الطاقة المحسوب لنموذج psd في اتفاق معقول مع النتائج التجريبية عند أدنى نطاق طاقة (مستويات التكافؤ الإيجابية) ، بينما تظهر الحزمة الأعلى (مستويات التكافؤ السالب) قيمة أكبر من البيانات التجريبية بحوالي 12-2 MeV

يتكون حساب نموذج القشرة المستخدم للتوسعة بدون وجود لب من أربع قشر هي(1s، 1p، 1d-2s، 1f-2p) مقطوعة إلى $\hbar\omega$ (0 + 2) وهو ما يكفي من التقارب لهذه الحالات لأن التوسعة إلى 4 و 6 يعطي فقط تغيير طفيف في قيمة الطاقة للمستويات العليا فقط. تتفق حسابات التوسعة بدون لب لمستويات الطاقة السفلى بشكل جيد مع النتائج التجريبية لكلا النواتين.

تم حساب عوامل الشكل المرنة وغير المرنة لحالة الإثارة المنخفضة لكلا النوى باستخدام جهد سكايرم (sly4) والتي تُظهر توافقًا جيدًا مع البيانات التجريبية مقارنةً بحسابات جهد وود- سكسن.

جمهورية العراق

وزارة التعليم العالي والبحث العلمي

جامعة كربلاء

كلية العلوم

قسم الفيزياء

دراسة التركيب النووي للنوى الخفيفة

(^{6}Li , ^{9}Be)

رسالة

مقدمة الى قسم الفيزياء في جامعة كربلاء وهي جزء

من متطلبات نيل شهادة الماجستير في علوم الفيزياء

تقدمت بها

سبأ مجيد حميد

اشراف

أ.د. عدي داود سلمان

٢٠٢١ م **١٤٤٢ هـ**